Politecnico di Torino

Politecnico di Torino
Environmental and Land Engineering
A.y. 2022/2023
Sessione di Laurea Marzo 2023

Microseismic monitoring of rock glacier activity: a case study on Gran Sometta Rock Glaciers (NW Italy)

Supervisor:
Chiara Colombero

Candidate:
Lorena Di Toro

CONTENTS

LIST OF FIGURES

LIST OF TABLES

ACKNOWLEDGMENTS

I would like to express my gratitude to Professor Chiara Colombero for imparting her passion for the subject of my thesis and supporting me throughout the entire process. Her guidance and feedback have been fundamental in shaping my work and ensuring its quality. Thank you, Professor Colombero, for your dedication and encouragement.

I would like to express my gratitude to Turin, not just as a city, but for what it represents to me. It came into my life at the right moment and was a breath of fresh air, even though it was 800 km away from my home. This was made possible by the wonderful people I have found here.

Thank you Vale and Edo for being the best friends I could have found here, I am grateful for your presence in my life. And to Lolla, thank you for bringing positivity and energy during a time when we needed the most.

Thank you Matteo, Giulio and Marco for making me feel a little bit closer to Abruzzo even when I am here. Your friendship has been a source of comfort and familiarity in a new place, and I am grateful for the memories we have shared together.

Thank you Bruno for always believing in me and for supporting me throughout this journey.

I would also like to thank my sister for being such an inspiration to me and for pushing me to grow and overcome my limits.

I am extremely grateful to my mother, for her constant support and guidance throughout my life. She has been a pillar of strength, always ready to help me and provide words of encouragement. This graduation is for you.

1 ABSTRACT

Fracturing, stick-slip movements, water flow, seepage and other natural events related to the glacial and periglacial environment release energy in the form of elastic waves, also known as microseismic events. Microseismic activity represents therefore a useful tool to study glacier dynamics as it can provide information about their mechanical and structural variations. For this reason, a network of passive seismometers has been installed on the Gran Sometta rock glacier (Aosta Valley, NW Italy) since July 2020 to continuously record ambient seismic noise and detect microseismicity.

As a first step of this study, microseismic signals generated in and around the glacier have been detected in the continuous noise recordings through a short-time-average over long-time-average (STA/LTA) algorithm. It was applied directly on the raw signals after the setting of some key parameters (STA window length, LTA window length, pre-event window, post-event window etc.).

The second part of the study was the classification of the detected events. It was performed in two ways: visual analysis of the event spectrograms and cluster analysis on four key time- and frequency-domain parameters. These are kurtosis, bracketed duration, 5-Hz frequency class containing the highest energy amount and peak frequency of the amplitude spectrum. The visual classification led to the recognition of six types of recurrent events*:* low frequency and long duration events (below 10 Hz, tens of seconds), earthquakes, rockfalls, rain-related noise events, snow-related events, high frequency and short duration events (in the range 10-40 Hz).

Events characterized by very high frequencies and long durations were removed from the dataset since they were found to be mostly related to the rainfall seismic signatures and other events occurring in the rock glacier surroundings. This filtering procedure allowed to get a more stable clustering of the events likely related to the rock glacier internal processes. The automatic classification of the remaining events was then conducted through a k-means clustering algorithm. The latter was selected since the only required input is the number of desired clusters. Initially, four clusters were defined on the basis of the visual classification but through a trial-and-error procedure, the number of sub-clusters was increased to 8 to better describe the dataset.

The seasonal trend of these classes was then computed and compared to meteorological parameters of the site (air temperature and precipitation) to get a more complete interpretation of the different processes involved.

Similarities among the seasonal and hourly occurrence of these 8 classes were found and this allowed to combine the 8 sub-classes back into 4 main clusters, including i) low frequency deep quakes (likely related to the rock glacier basal movements); ii) high-frequency shallow quakes (likely icequakes and other processes related to the seasonal modifications in the rock glacier active layer); iii) snow-related events (likely due to a stress redistribution on the rock glacier due to the presence of a high snow cover) ; iv) residual hybrid events still related to rain and other high-frequency short duration quakes.

The analysis of the temporal rate of the different clusters may provide a valuable monitoring tool for the rock glacier activity and internal processes.

2 INTRODUCTION

2.1 MICROSEISMIC APPLICATIONS

Microseismic monitoring is a passive seismic method that finds potentially widespread application in climate change mitigation, monitoring and adaptation efforts. The word "passive" means that these methods use recording-capabilities only and no input is required from the user, in contrast with common active seismic methods for which seismic sources are required to illuminate the subsurface.

The monitoring involves the recording of seismic signals, commonly referred to as ambient seismic noise or ambient vibrations, which are characterized by a low frequency content. Indeed, the frequency range of application of these systems is generally below 100 Hz.

The ambient vibrations are generated by natural phenomena, such as winds, oceanic waves, rivers, earthquakes and icequakes, as well as by anthropic disturbances like traffic and industrial noise. All these sources can be exploited to retrieve information about the investigated subsurface. In particular, microseismic (MS) events related to the target of interest can be extracted from the continuous ambient seismic noise recordings through detection algorithms. Their classification, temporal rates and source locations can provide valuable information about the investigated processes.

Therefore, one of the main advantages of microseismic monitoring is that it is a completely non-invasive technique. In fact, it does not require the use of active seismic sources such as guns, hammers, and explosives to generate the seismic signal, as the recorded signal is naturally occurring. This feature makes it even a more attractive option when dealing with remote sites or environmentally sensitive areas.

Regarding the applications of microseismic monitoring, it can be used to study the effects of climate change on the stability and movement of glaciers, permafrost and rock mass settings.

One of the well-known effects of climate change is the warming and thawing of **permafrost**. When permafrost melts, it can lead to alterations in ground stability and water movements in the subsurface. Recently, passive seismic monitoring has been used to observe freeze-thaw processes of permafrost. These processes can cause rock detachments in permafrost areas that may pose a potential hazard to infrastructure and settlements. Linder et al. (2021) conducted a study on microseismic events at Mt.

Zugspitze in Germany, in which they analysed passive seismic data to obtain seasonal seismic velocity changes and velocity decreases in the area of interest. They also compared the results with meteorological data, suggesting that seasonal freeze-thaw cycles and permafrost degradation contribute to these velocity variations.

In addition, MS monitoring can be employed to investigate the effects of climate change on the stability of rock mass settings such as volcanic edifices, lahars, debris flow and ice-avalanches. In relation to **rock-slope stability**, microseismic activity can be useful to evaluate damage and cracking processes that may be indicative of macroscopic failure. More precisely, MS events associated with fractures can provide information about acceleration to failure and identification of the unstable compartments and slip surfaces, as demonstrated by Senfaute et al. (2009). They analysed microseismic events detected prior to the collapse of a coastal cliff sector in Normandie and established that MS signals are useful to understand incipient failure of internal rock bridges. Then, they also found a correlation between seismic events, displacement-rate measurements and climatic parameters.

More precisely, variations in air temperature or temperature differences on the rock mass can induce thermal dilation and thermal stresses leading to microcracking processes, as demonstrated by Colombero et al. (2018). The authors performed a microseismic study of an unstable granitic cliff located in north-western Italian Alps (Madonna del Sasso, VB), in order to assess its stability and the correlation with climate data. They found peaks of microseismic activity during summer, likely related to the rock mass thermal expansion, and low daily rates during colder periods.

The correlation between seismic events and rainfall is another field that is continuously investigated in the literature. Rainfall is often found to be a triggering factor for rockfalls and microseismicity occurrence. As a matter of fact, Helmestetter et al. (2010) demonstrated that rockfall activity increases immediately during a rainfall event and lasts several days after through a seismic study on Sèchillienne rockslide (French Alps). Rain also induces strong accelerations of the rockslide movement and then peaks in microseismicity.

Another field of application for MS technology is **rock engineering**, specifically in mines, underground powerhouse and deep tunnels. It is clear that rock excavation results in stress modification of rocks in the surrounding area, leading to cracks generation and energy release. To address these issues, Ruochen Jiang et al. (2020) used MS sensors to capture signals released by rock fracture. By analysing the signals, they were able to obtain parameters such as occurrence time, source location and intensity that were useful for early warnings of possible hazards, such as rockbursts.

Microseismic monitoring is a valuable technique also for a wide range of applications related to climate change mitigation, including Carbon Capture and Storage (CCS) systems and renewable energies.

CCS is a technology that involves capturing carbon dioxide emissions and storing them underground in geological formations to prevent their release into the atmosphere. The goal is to reduce greenhouse gas emissions, which contribute to climate change.

CCS technology is still in the early stages of development, and there are some technical challenges that need to be addressed. These challenges include the potential risk of inducing earthquakes during the injection process.

As a matter of fact, seismic monitoring is an important tool for ensuring the safe and effective deployment of carbon capture and storage projects. It is used to detect and analyse vibrations in the Earth caused by activities such as drilling, CO_2 injection, increasing pore pressure of the formation and re-activation of pre-existing faults that may lead to CO_2 leakage.

However, geomechanical response to injection can vary significantly based on the geological setting. For instance, Stork et al. (2015) found that injection activities triggered a deep fracture zone in In Salah CO_2 storage. The installation of geophones on the site helped them to identify that the rate of these events increases when the injection rate exceeds a certain threshold.

As previously said, microseismic monitoring is also used in renewable energy applications, such as geothermal energy. This form of energy can be used to generate electricity or provide heat for industrial processes and building heating purposes.

Albaric et al. (2014) showed that more than 7000 induced microearthquakes were recorded during the stimulation of a geothermal reservoir. As a matter of fact, the possible causes of induced seismicity in geothermal areas are pore pressure change, thermoelastic stressing due to temperature changes, excavation-related stresses, chemical changes of fault properties and dynamic triggering.

2.2 MICROSEISMIC APPLICATION FOR ROCK GLACIERS MONITORING

Climate change is having a significant impact on glaciers and rock glaciers around the world. Glaciers are melting at an unprecedented rate, with significant mass loss and rapid retreat. This is primarily due to increasing global temperatures, which are causing the ice to melt at a faster rate than it can be replenished by rainfall.

For these reasons, the study of local targets, such as mountain or alpine glaciers and rock glaciers, is gaining more and more importance in recent years.

Rock glaciers are creeping landforms of ice and rock debris. Due to their small size and peculiar structure, they are highly sensitive to changes in temperature and precipitation, and thus represent key features to understand the response of the glacial and periglacial environment to climate change. This latter, and in particular the increase of air temperature, strongly influence the thermal state of permafrost.

The external characteristics of the rock glacier (topographical conditions) and the internal ones (i.e., internal structure and composition), together with ground temperature control perennially frozen ground deformation and the associated glacier flow velocities.

Variations of these features may lead to destabilization and collapse of the rock glaciers, making these targets not only useful for climate change evaluation and monitoring, but often an issue in the light of climate change adaptation. These targets are indeed showing evidence of high instability with the ongoing climate modifications, with potentially serious consequences and melting-related natural hazards. Destabilization events are characterized by high horizontal velocities, high front advance rates and crevasse-like cracks opening. As demonstrated by Delaloye et al. (2012), the main causes of rock glacier destabilizations are:

- morphological forcing (steep slope angle, higher shear stress, convex bedrock topography, local thinning of the glacier);
- mechanical forcing due to external factors (landslides, rock avalanche and rockfalls);
- thermal forcing and increasing pore water pressure.

All these events may increase the rate of mass wasting at the front of the rock glacier and change its geometry. On the contrary, torrential and debris flows can increase the hazard related to rock glaciers. However, these variations related to the internal glacial processes release energy in the form of elastic waves, also known as microseismic events.

For this reason, microseismic monitoring has become a useful tool to assess changes in rock glacier properties at depth and to characterize the damage and destabilization processes.

Seismic monitoring of glaciers involves detecting, locating and characterizing seismic activity induced by several phenomena such as rock falls, debris flows, crack propagation, basal sliding or melt-water runoff. The different mechanisms of deformation can be discriminated using the properties of seismic events such as frequency, duration, location and temporal distribution, as performed by Gulliemot et al. (2020) who conducted a passive seismic study on Gugla rock glacier, in Switzerland. Based on duration and frequency, they classified the microseismic signals into quakes and rockfalls and analysed their seasonal occurrence, demonstrating that bursts of microseismicity took place during melting periods, such as during the spring.

Short and impulsive signals with frequencies within the 10 – 40 Hz range are generally indicative of small crack formation and propagation. Conversely, long and complex signals characterized by high amplitude are likely attributable to serac collapses (Roux et al., 2008).

Furthermore, low frequency events may also be a manifestation of increasing fluid flow within the glacier, whereas high frequency signals can be correlated to water pressure increase that changes the stress distribution in the glacier.

2.3 THESIS OBJECTIVE

The primary objective of this thesis is to conduct a microseismic survey to investigate the dynamics and internal processes of the Gran Sometta rock glaciers located in the upper Valtournenche Valley (Aosta Valley, NW Italian Alps).

To achieve this goal, a network of four passive seismometers (GEA2 – GEA5) was installed on the rock glacier (**Figure 1**) in July 2020. Ambient seismic noise was continuously recorded on site for a long period (more than one year) with a sampling frequency of 250 Hz. One of the main aims of the microseismic network is to detect the microseismicity related to the rock glacier processes.

The study is divided into three phases:

1. Detection of microseismic signals embedded in the continuous ambient seismic noise recordings;

2. Classification of the detected events using visual (manual) and clustering (automatic) analysis;
3. Interpretation and comparison of the resulting clusters with meteorological parameters.

The aim of the first step is to detect the microseismic signals, separating them from the rest of the recordings. This is accomplished through a short-time average over long-time average (STA/LTA) algorithm, widely used in seismological applications.

In the second part of the thesis, the detected signals are classified integrating two modalities: visual analysis of the events spectrograms and clustering analysis on key time- and frequency-domain parameters.

To conduct the visual classification, a MATLAB script is utilized to obtain the seismogram, Fourier spectrum and spectrogram for each detected event.

In order to carry out the clustering analysis, first a semi-automatic procedure is applied. As a matter of fact, eleven different parameters will be computed for each extracted event, drawing upon the research conducted by Hibert et al. (2014).

These parameters include maximum amplitude over the mean amplitude, kurtosis, bracketed duration, uniform duration, total time of the event, increasing time to decreasing time, 5-Hz frequency classes containing the maximum energy peak frequency, maximum amplitude on the N component and the ratio of maximum amplitude to the bracketed duration.

After computing the eleven parameters, a trial-and-error procedure is used to select the most relevant ones for the cluster analysis. This latter is performed applying the k-means algorithm, since the only input needed is the number of desired clusters.

The classification outcomes provide valuable information about the types and characteristics of the microseismic events.

The final step of this thesis involves a comparison of the obtained classes with meteorological parameters. This analysis is useful to investigate the occurrence of each class and to understanding any correlation with climate data. By identifying the occurrence of a class during a specific season or in a particular meteorological scenario, this study may help in determining whether environmental factors trigger certain cluster events that may be related to inner processes of the rock glacier.

3 TEST SITE AND MONITORING NETWORK

Gran Sometta is located on the south-western side of the central Alps, at the head of the Valtournenche Valley (Aosta Valley, Italy). It is a landform classified as a rock glacier and it is characterized by two distinct lobes with elevations ranging from 2630 to 2770 m in the frontal area. It is approximately 400 m in length, between 150 and 300 m wide and exhibits a thickness of 20-30 m, estimated from active geophysical investigations, such as electrical resistivity tomography and seismic reflection. Additionally, a third lobe is present, with its front located at an altitude of approximately 2700 m a.s.l, measuring 215 m in width and 192 m in length.

Since 2012, Gran Sometta has been under investigation for the purpose of evaluating its flow rates. Indeed, it has been selected by the Regional Agency for Environmental Protection (ARPA Valle d'Aosta) as a long-term monitoring site of permafrost degradation and response to climate change. The ski resort of Cervinia and the Goillet Lake (which spans over an area of 0.48 km^2, with a maximum depth of 37 m) are located downstream the rock glacier flow, posing additional concern on possible collapses and fluidification of the ice and debris material.

As a matter of fact, the interannual fluctuations in creep rates of the rock glacier permafrost are consistent with the observed trend in other Alpine glaciers. Between 2012 and 2020, the maximum peak surface velocities were reached in 2015 (0.21 – 1.45 m/y), with subsequent deceleration in velocity until 2017 – 2018. However, over the following two years (2019 and 2020) the surface velocity exhibited a gradual increase reaching values of 0.23 cm/y up to a maximum of 1.9 m/y (Bearzot et al., 2022).

Figure 1 shows the location of the study site.

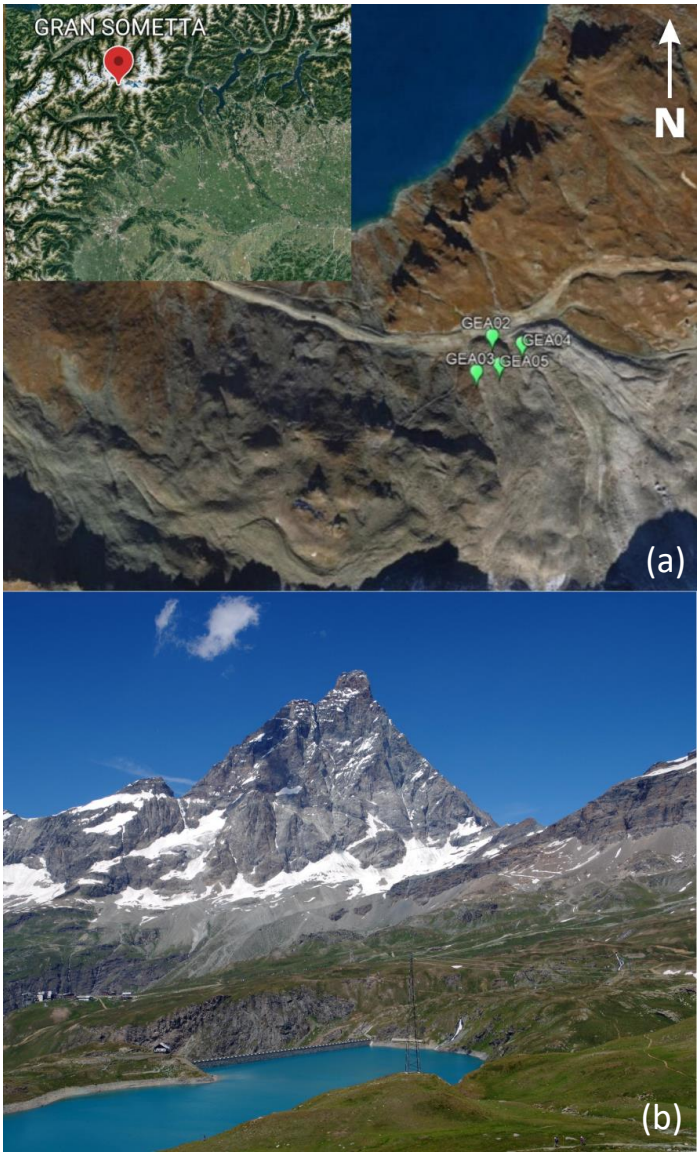

Figure 1. *(a) Geographic location of the study site (Gran Sometta), in south-western side of the central Alps. (b) View of the Goillet Lake from the rock glacier.*

For these reasons, a network of four wireless passive monitoring stations (GEA2-GEA5 in **Figure 2**) was installed on site in July 2020 to continuously record ambient seismic noise.

Each station is composed of a 2-Hz triaxial high-sensitivity geophone (200 V/(m/s)) and a digitizer / recorder (GEA-GPS, developed by PASI s.r.l. and Iridium Italia s.a.s.) as shown in **Figure 2**.

These instruments have guaranteed continuous seismic noise recording at 250 Hz sampling rate, low-weight to reach remote areas, low power consumption and daily remote information about the system by a GSM-GPRS module.

Synchronization between the monitoring system was provided by GPS timing. Data are stored in 1 h files in an internal 32 GB memory card.

Figure 2. *Instruments for the monitoring network.*

Two monitoring stations, GEA2 and GEA5 (**Figure 3**), were installed on the black lobe of the glacier. A third station, GEA04, was installed on the white lobe. Additionally, a reference station, GEA03, was installed outside of the lobes.

***Figure 3**. Geometry of the monitoring network.*

In the following table the coordinates of the seismic stations are reported.

***Table 1.** Location of seismic monitoring stations (GEA2 – GEA5).*

STATION	X [m]	Y [m]	Z [m]
	WGS84 UTM32N	WGS84 UTM32N	GPS
GEA02	396704	5086284	2654
GEA03	396672	5086215	2661
GEA04	396762	5086268	2660
GEA05	396717	5086228	2667

4 METHODS

The methodology employed in this work is based on the detection, classification and interpretation of recorded events at the monitoring stations (GEA2 – GEA5) during a monitoring period of more than one year (July 2020 - September 2021). Few data gaps are present due to insufficient power supply at the monitoring stations.

Figure 4 summarises the main steps of the methodology developed and followed in this thesis.

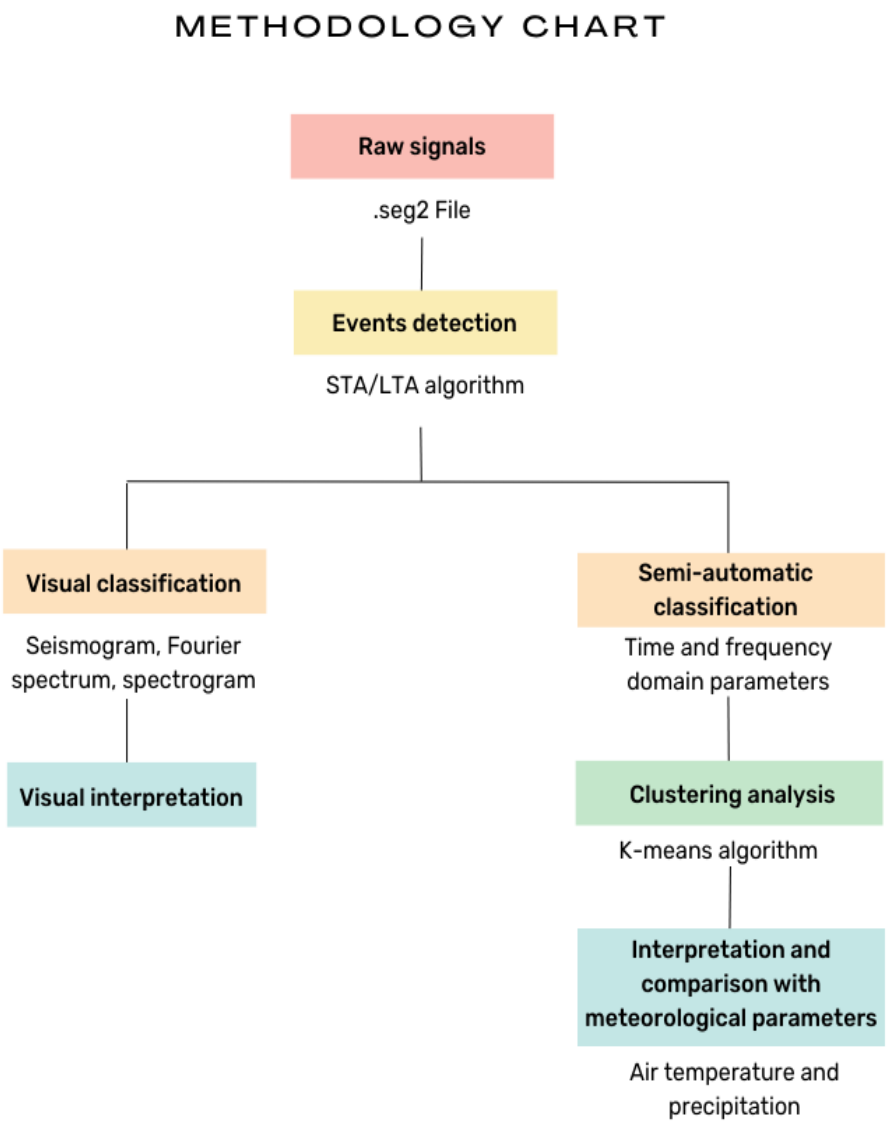

***Figure 4**. Workflow of this study.*

4.1 EVENTS DETECTION

The detection of microseismic events was accomplished using a Short Time Average to Long Time Average (STA/LTA) detection algorithm, which is the most used approach in seismology for event detection.

This algorithm is able to filter seismic signals in consecutive moving-time windows: a short-time average window (STA) and a long-time average window (LTA). The STA approximates the instant amplitude of the seismic signal, the LTA represents the average seismic noise amplitude.

The algorithm calculates the absolute amplitude of each data sample of the incoming signal and determines the average of absolute amplitudes in both windows. Subsequently, the ratio of these two values (STA/LTA ratio) is computed.

An event is detected when this ratio exceeds a user-predetermined threshold. The optimal threshold value for detecting events, called *STA/LTA trigger on threshold*, depends on the seismic noise condition and on the tolerance to false-trigger events. Therefore, it is advisable to use a high value of the ratio to detect fewer false-trigger events. In quiet areas, the ratio can conversely be kept low.

The STA/LTA trigger on threshold is not the only parameter to set in order to apply the algorithm, but also:

- STA window duration (in s)
- LTA window duration (in s)
- Pre-event window (in s)
- Post-event window (in s)
- STA/LTA trigger off threshold level (-)

Their selection depends on several factors including the objective of the study, the seismic noise condition at the site, the properties of seismic signal at a given location and on the type of sensor used.

More precisely, the *STA duration* should be longer than a few periods of the expected seismic signal but shorter than the expected shortest events, to ensure that the average operates effectively.

The *LTA window* should be longer than a few periods of typical seismic noise fluctuations. Changing its value, the recording may be more or less sensitive to regional events. A longer LTA window increases the trigger sensitivity to earthquakes, whereas a shorter LTA window improves the recorder sensitivity to man-induced seismic noise.

The *STA/LTA trigger off threshold level* is also crucial as it determines the termination of data recording and the capture of coda waves. A low value is recommended to include as much of the coda waves as possible. However, an excessively low level may result in very long records.

The algorithm's ability to capture the signal during an event is limited to when the waves with the maximum amplitude reach the station, rather than at the beginning.

To address this issue, a *pre-event window* is considered. It assures that the entire event is recorded.

Similarly, the *post-event window* has the same purpose: it is used to capture the remaining coda of events that is smaller than the STA/LTA trigger off threshold.

Additionally, it is possible to define a window length to skip after the STA/LTA threshold is exceeded, in order to avoid multiple detections of the same event.

The parameters applied in the algorithm adopted for this study are shown in **Table 2.**

Table 2. *Parameters used for event detection.*

STA/LTA parameters	
STA window length	0.5 s
LTA window length	10 s
Pre-event window	3 s
Post-event window	15 s
Skip after end of the event	0.5 s
STA/LTA trigger on threshold level	6
STA/LTA trigger off threshold level	1.5

The advantages of this method are that it is fast and can be used directly on raw signals. However, it requires careful setting of the above-mentioned parameters.

4.2 EVENTS CLASSIFICATION

The second step of the analysis was to classify the recorded events. It was performed integrating two options:

- Visual classification;
- Semi-automatic classification.

The **visual classification** approach relied on the observation of event spectrograms, which provide a graphical representation of the frequency spectrum of a signal over time.

As an example, microseismic events related to fracturing are impulsive and short duration signals characterised by a triangular shape with a clear coda in the time domain. These events can occur as single isolated events or in sequences with varying time intervals.

The spectrogram of a microseismic event typically exhibits a sharp energy increase followed by an exponential decay of high-frequency content over time (**Figure 5**). The maximum amplitude of the event is variable, and, in some cases, the high-frequency content is partially or totally missing.

Due to these peculiar features, these events can be easily recognized by the user with visual classification. The method has the advantage of being completely user-controlled, but the main disadvantages of being potentially subjective and depending on the observer. In addition, it might become time-consuming with big datasets of thousands of events. If the monitoring network has early warning purposes, this approach cannot be applied in near real-time.

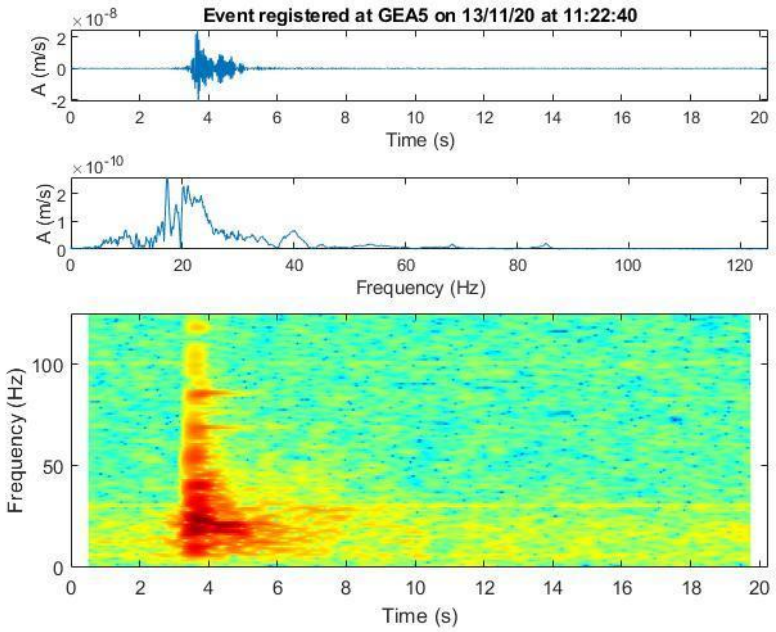

Figure 5. *Example of a microseismic event recorded at GEA5 station. From the top to the bottom: seismogram recorded on channel N of GEA5, related Fourier spectrum and spectrogram.*

The **semi-automatic procedure** had the aim to transform the seismic-signal characteristics into objective criteria. These criteria must be both discriminating and simple enough to ensure a fast and reliable computation.

For these reasons, a matrix containing ten time- and frequency-domain signal parameters has been calculated using MATLAB.

These parameters are:

- Ratio of the maximum to the mean amplitude of the signal in time domain;
- Kurtosis;
- Bracketed duration;
- Uniform duration;
- Total time of the extracted event;
- Duration of the increasing and decreasing phase of the signal;
- 5 Hz frequency classes with the maximum energy content;
- Peak frequency;
- Maximum amplitude on one of the three components (e.g. N);
- Ratio of the maximum amplitude to the bracketed duration.

All these parameters were computed to find the most sensitive for the classification of the detected events.

However, after this preliminary analysis, the cluster analysis was based on four of these parameters: *kurtosis, bracketed duration, 5-Hz frequency class with maximum energy and peak frequency.* These four parameters were indeed found to have the largest variations between different recorded events.

Kurtosis is a statistical parameter that characterizes the shape of a given distribution (a normal distribution has kurtosis equal to 3). Therefore, it corresponds to a measurement of the flatness or peakedness of the distribution. In seismic applications, low kurtosis values are indicative of ambient seismic noise recording and non-impulsive signals, while high kurtosis values are related to sharp impulsive seismic signals.

The *bracketed duration* parameter represents the time interval between the first and last samples exceeding a threshold equal to 20% of the signal maximum amplitude.

The Peak frequency refers to the frequency at which the signal has its highest amplitude in the frequency domain. It is typically identified through the peak in the frequency spectrum of the signal.

The *5-Hz frequency classes* with maximum energy are related to the event spectrum. Indeed, the spectrum can be divided in 5 Hz frequency classes (5-10 to 95-100 Hz) to identify the frequency range having maximum amplitude.

Afterwards, ***k-means*** clustering was applied. This algorithm is widely used for clustering large datasets, and it is able to classify a set of n-dimensional observations into k different clusters, where k is a subjective parameter and the only required input for the algorithm.

First, the algorithm randomly selects k centres, then it assigns each observation to the nearest center (computing the distance in n-dimensions), recalculating the cluster centroid after each assignment.

The iterative process continues until the cluster assignments do not change anymore or a maximum number of iterations is reached.

The Euclidean distance is used to determine the distance between each data object and the cluster centres. Considering two vectors $x = (x_1, x_2...x_n)$ and $y = (y_1, y_2...y_n)$, the Euclidean distance $d (x_i, y_i)$ is obtained as follow:

$$d\ (x_i, y_i) = \left[\sum_{i=1}^{n} (x_i - y_i)^2\right]^{1/2} \qquad (1).$$

Thus, the only input needed are the number of desired clusters, *k*, and a dataset containing n observations.

The steps performed by k-means are better explained below:

1. Random selection of *k* data objects from the data set as initial cluster centres
2. Repetition of point 1
3. Calculation of the distance between each data object n_i *(1 ≤ i ≤ n)* and all *k* clusters c_j *(1 ≤ j ≤ k)* and assignment of observation n_i to the nearest cluster
4. For each cluster *j (1 ≤ j ≤ k)*, recalculate the centroid until no change in the center of clusters is obtained.

5 RESULTS

5.1 EXTRACTED EVENTS

The total number of extracted events from the original data set (July 2020-October 2021) was 45326. Many events were recorded simultaneously at the four stations, while the majority of them were recorded by a lower number of stations.

In **Table 3**, the number of recorded events and the reference monitoring period are summarized for each station.

Table 3. *Number of detected events for each monitoring station (GEA2 – GEA5).*

Station	Number of events	Monitoring period
GEA2	7884	21 July 2020– 4 August 2021
GEA3	19996	21 July 2020 – 5 October 2021
GEA4	8308	21 July 2020 – 4 September 2021
GEA5	9138	21 July 2020 – 4 October2021

It is important to note that the monitoring periods for each station are different, and this may affect the number of events recorded. The station with the longest monitoring period is GEA3, which recorded the highest number of events (19996). This station is located outside the lobes, on a slope characterized by debris and rock falls, which may explain why it recorded more events than the other stations.

However, it is also interesting to note that the stations with shorter monitoring periods (GEA2 and GEA4), still recorded a significant number of events (7884 and 8308, respectively).

5.2 VISUAL CLASSIFICATION ANALYSIS

The visual classification is based on the analysis of the results obtained from a MATLAB code able to display events in three graphs:

- The seismogram for the whole duration of the event;
- The Fourier amplitude spectrum;
- The spectrogram, i.e. frequency content variations over time.

The seismogram is a graph that plots the amplitude (in m/s) of the seismic waves over time (in s, time domain). The Fourier amplitude spectrum is a way of representing a signal in terms of its frequency components (frequency domain): the signal is decomposed into a series of sinusoidal components of different frequencies, each with its own amplitude. This allows to analyse the frequency content and identify the frequencies that are present.

The spectrogram of a seismic signal is a graphical representation of the frequency content of the seismic waves over time (time and frequency domain). It is a time-frequency analysis tool that provides a more detailed view of the seismic signal compared to the seismogram.

After conducting a comprehensive analysis of these figures, six primary categories of events have been distinguished.

The first class is composed of events with very low frequencies and long durations (around 10 s) with a slowly emerging signal. The Fourier spectrum associated with this class is marked by intense peaks that lie below 10 Hz while the spectrogram is characterized by a persistent low frequency band (**Figure 6**).

Due to the frequency and duration characteristics, these events may be associated to the basal movements of the rock glaciers and/or the slip of the materials along pre-existing fractures.

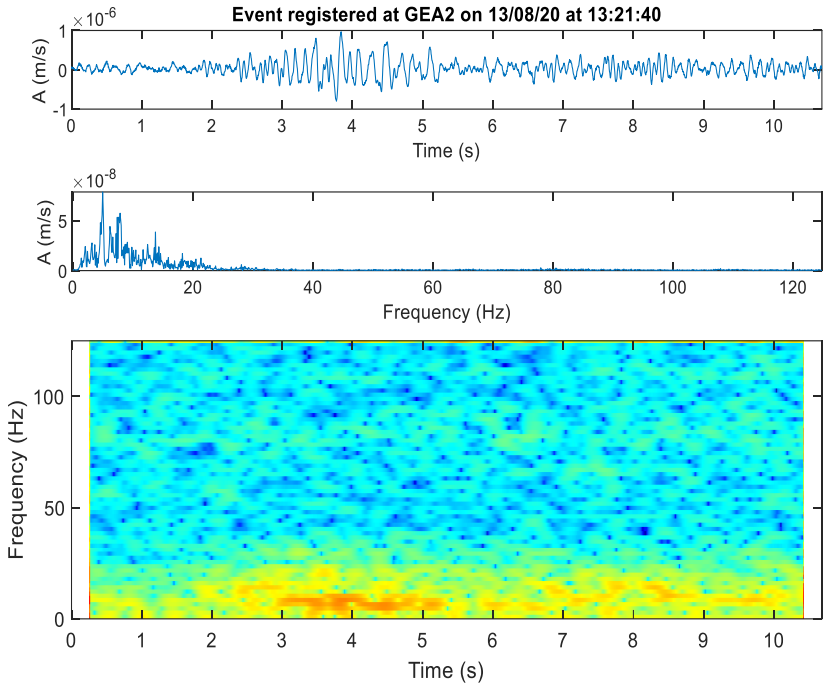

Figure 6. *Seismogram, Fourier spectrum and spectrogram of a typical event belonging to the first (visually recognized) class, registered at GEA2 on 13/08/20.*

Another class of recurrent events is characterized by higher frequency content in the Fourier spectrum (between 10 and 30 Hz) with respect to the first class and short duration (typically few seconds). The spectral data show a clear high-frequency emerging onset followed by an exponential decay of the high frequency content with time.

This class of events may be associated with variations of the active layer of the rock glaciers or with micro-cracking and micro-fracturing processes as indicated by Colombero et al. (2018). The frequency content of these signals depends on the size and distance of the source, but independently from the source, they are always characterized by the strong and fast attenuation of the high frequencies. Based on the available information, it is possible to classify these events as "quakes".

In **Figure 7**, an example of event belonging to this class is shown.

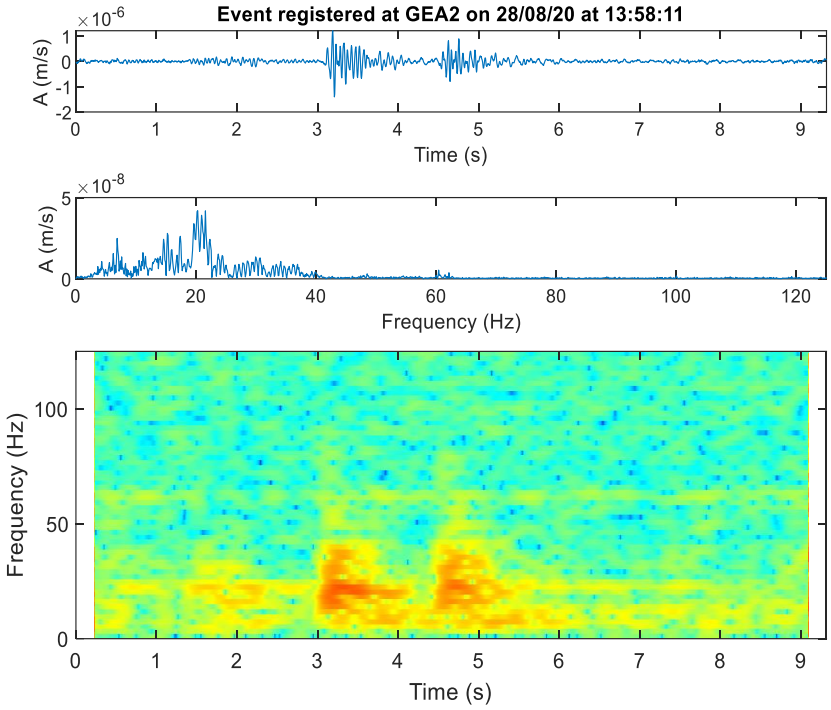

Figure 7. *Example of series of two short events belonging to the second class registered at GEA2 on 28/08/20. From top to bottom: seismogram, Fourier amplitude spectrum and related spectrogram.*

On the contrary, events belonging to the third class reach the highest energy at around 40 Hz, potentially accompanied by additional peaks at 60 and 80 Hz. These events tend to last for roughly 20 s.

It is possible that this class is related to compaction or melting of snow, leading to stress alterations within the glacier. An illustration of an event related to snow is presented in **Figure 8**.

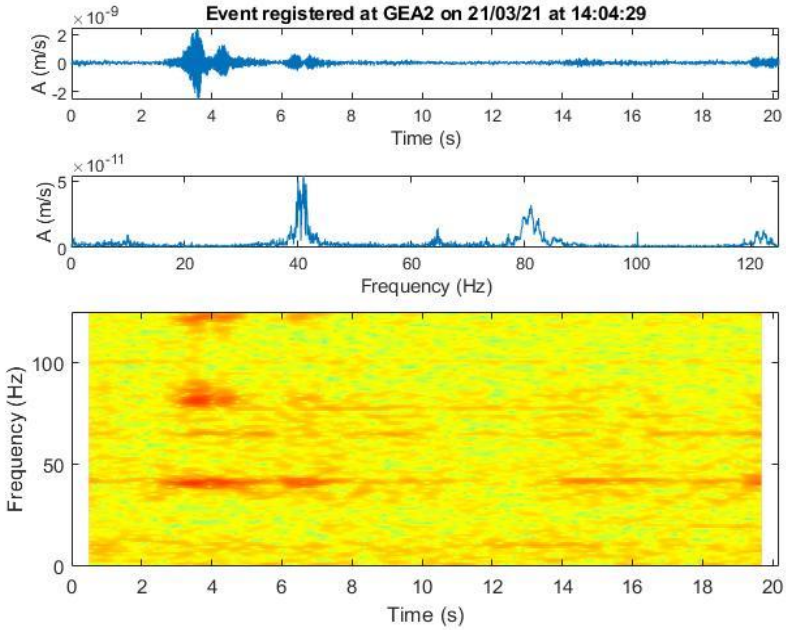

Figure 8. *Example of third-class event probably due to snow compaction, registered at GEA2 on 21/03/21.*

Events of the fourth class have long durations (around 20 s or more) and significant variations in the frequency content in time. Smaller events have the highest energy at 20 – 30 Hz. These features are typical of rockfall events, as studied by Helmstetter et al. (2010). The recorded signals may exhibit multiple subsequent peaks, which may be attributed to successive rock impacts.

The differences in frequency content can be explained by differences in the material involved or by different propagation conditions. The low-frequency spectral content observed in some recorded signals may be attributed to the larger distance of these events from the recording stations while the short duration may be due to a too weak impact to be detected.

Two examples of such events are shown in **Figure 9**. In these cases, the highest energy is reached at approximately 30 Hz and the duration is around 20 s.

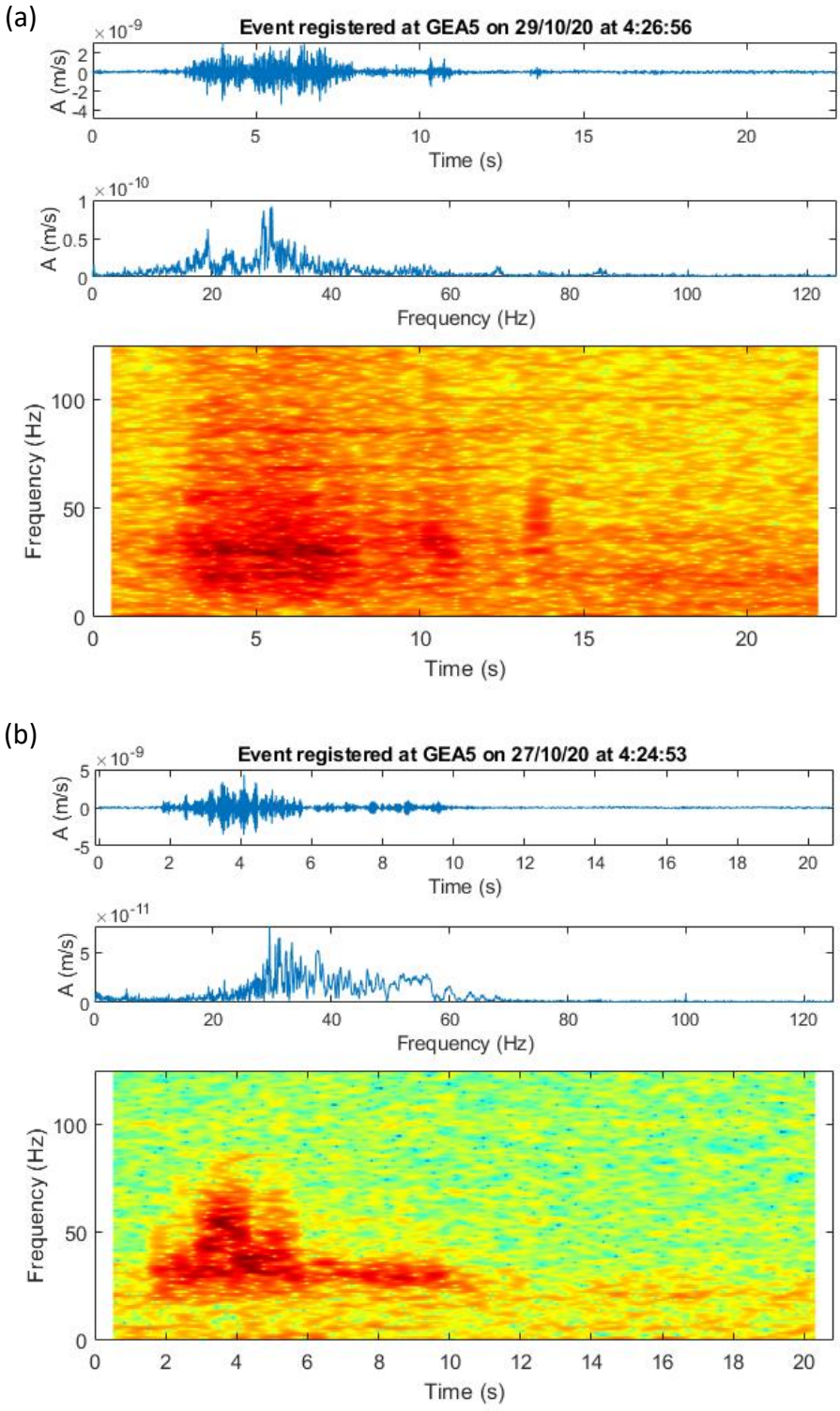

Figure 9. *(a-b) Example of fourth-class events. From top to bottom: seismogram, Fourier spectrum and spectrogram.*

The fifth class of events is represented by earthquakes. Although their occurrence is limited to less than ten events, their seismogram is easily recognizable since it is characterized by long durations and an impulsive signal. The Fourier spectrum of

these events displays low peak frequency, typically below 10 Hz, as visible in **Figure 10**.

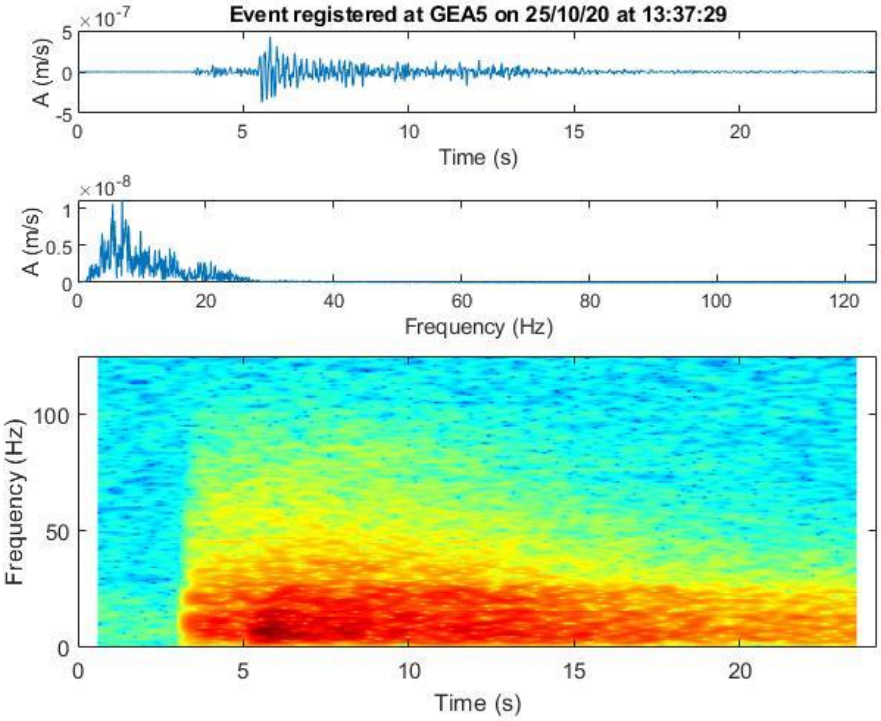

Figure 10. *Earthquake registered at GEA5 station on 25th October 2020 (depth = 1 km, M_t = 2.6). It lasts for approximately 20 s and the peak frequency is below 10 Hz.*

The final class of events have a spectrogram characterized by high amplitude vertical strips including a broad frequency band, generally above 60 Hz. This characteristic, along with the insights presented by Dean (2018), indicate that this class of events is associated with rain drops and infiltration close to the monitoring station.

An example of event related to rain is shown in **Figure 11**.

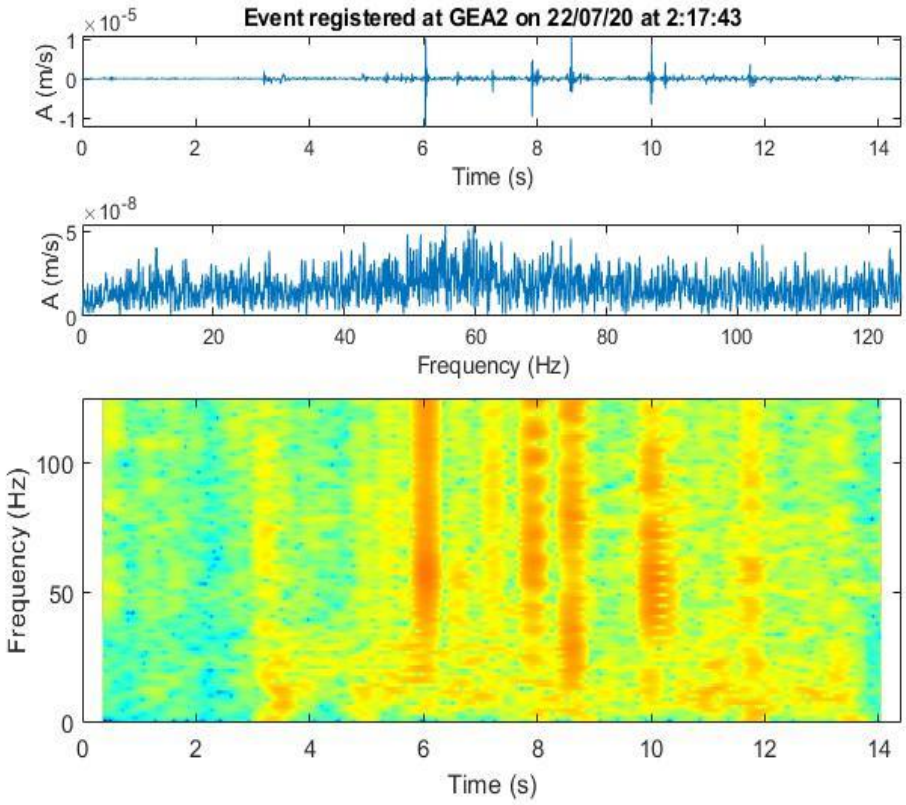

Figure 11. *Examples of events due to rain infiltration registered at GEA2.*

According to Dean (2018), rain represents a significant source of noise. The author demonstrated that when water falls directly on the geophone casing, the resulting noise is 30 times greater than when the water drops falls next to it. His study has also shown that even if seismic stations are buried, rain noise is not entirely attenuated. For these reasons, the events characterized by frequencies greater than 60 Hz have been removed before the clustering procedure to avoid interference from rain-related noise.

5.3 AUTOMATIC CLASSIFICATION

As previously said, the time- and frequency-domain parameters used in the clustering were kurtosis, bracketed duration, peak frequency and 5-Hz frequency classes with the maximum energy content.

These parameters were displayed for each station to check the existence of recurrent parameter values and their distribution over time. In this paragraph, the results of GEA2 station (front of the black lobe) are shown, while the results of the other stations (GEA3 to GEA5) are reported in Appendix A.

The peak frequency of the detected events over time, that was automatically picked from the event amplitude spectrum, is shown in **Figure 12a**.

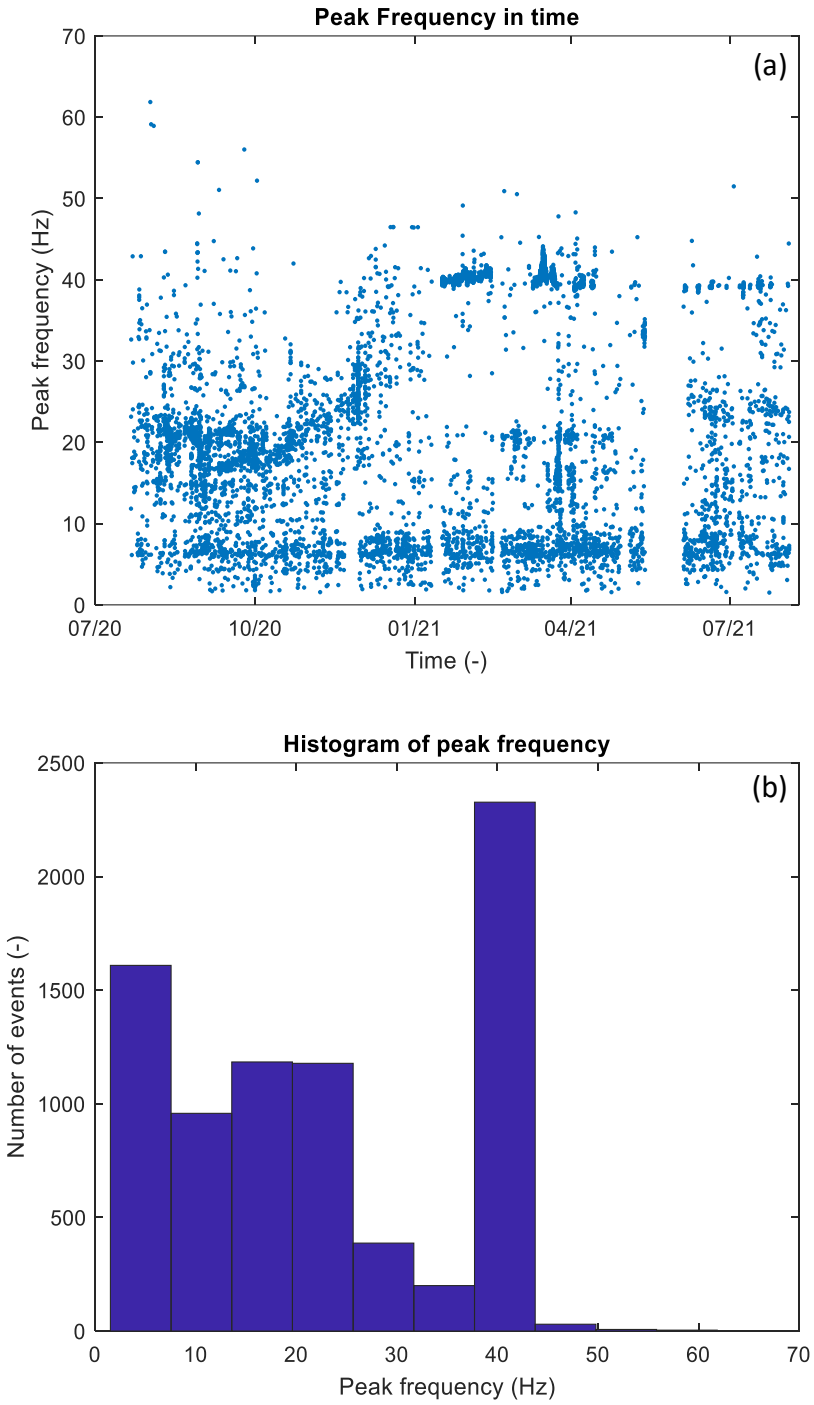

Figure 12. *(a) Peak frequency in time (b) Histogram of peak frequency of GEA2 station events.*

It is clear that most events (2330) have a peak frequency of approximately 40 Hz. These events are likely associated with snow compaction, as suggested in section 5.2. Additionally, there are many events that exhibit lower frequencies, including those with peak frequencies with peak frequencies below 10 Hz, which are related to the basal movements of the rock glacier or earthquakes (5.2). The remaining events are

characterized by peak frequencies that fall within the range of 10 to 45 Hz, while only a small number of events (41) exhibit peak frequencies greater than 45 Hz.

The second parameter analysed is the kurtosis. **Figure 13** displays the temporal variation of kurtosis for GEA2 events.

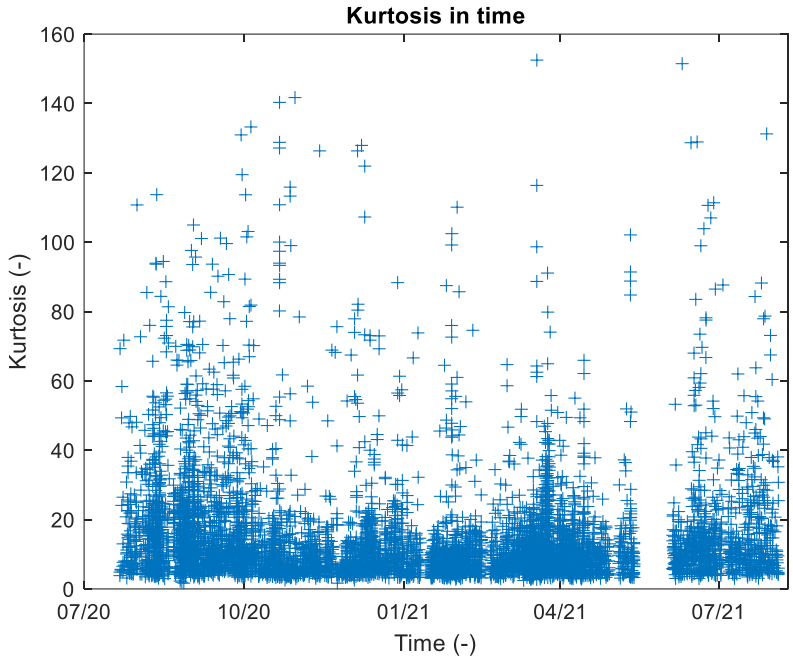

Figure 13. *Temporal variation of the kurtosis of GEA2 station's events.*

It is known that the kurtosis is a statistical parameter characterizing the shape of a given amplitude distribution (e.g., normal distribution has kurtosis equal to 3). In seismic applications, high kurtosis values are typically indicative of sharp and impulsive signals. As a matter of fact, most of the events of GEA2 station have kurtosis lower than 40 but there are also many events with very high values. Indeed, only 21 events are characterized by values lower than 3, so the distribution is defined as leptokurtic.

The third parameter is bracketed duration and its temporal evolution is shown in **Figure 14**. Except for sixteen events, the bracketed duration is always lower than 25 s.

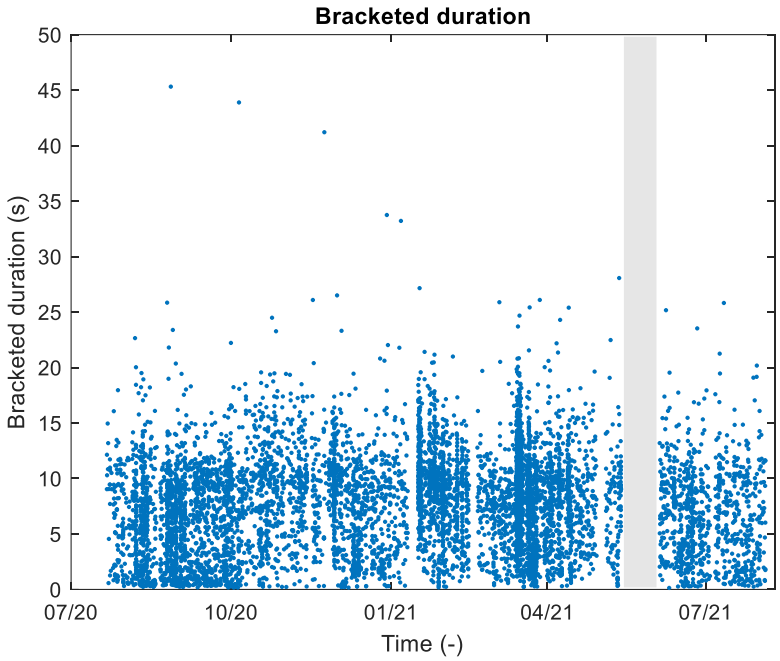

Figure 14. *Temporal evolution of bracketed duration of GEA2 station events.*

The last parameter is the 5-Hz frequency classes displaying the maximum energy content. This latter is useful to identify the frequency range characterized by maximum amplitude, and to verify if it is matching the peak frequency. The result is shown in **Figure 15**.

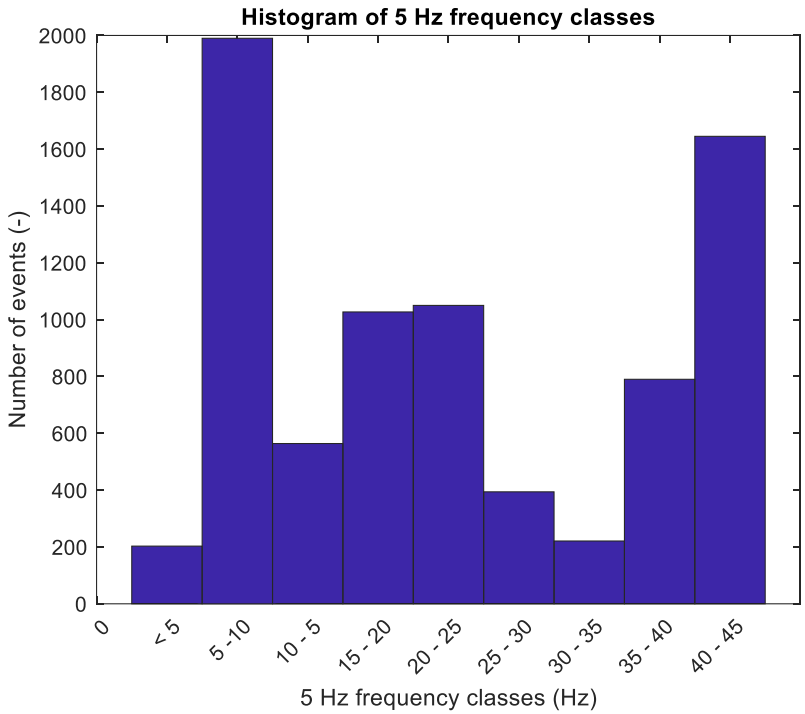

Figure 15. *Histogram of 5-Hz frequency classes containing the maximum energy amount of GEA2 station events.*

As visible in the previous graph, the frequency class with most events (1990) is 5-10 Hz followed by another class with events having frequencies between 40 and 45 Hz. In this case, the number of events that fall in this range is 1650. On the contrary, the classes with the least events are 0-5 Hz and 30-35 Hz.

5.3.1 K-means with 4 clusters

First, events with high frequencies and long durations were removed from the original dataset due to their likely relation to rainfall noise and other events occurring in the rock glacier surroundings. This filtering process, conducted using MATLAB, allowed to obtain a more stable clustering of events probably related to rock glacier internal processes.

Secondly, k-means cluster analysis was undertaken on the four classification parameters previously computed: peak frequency, bracketed duration, 5 Hz frequency classes and kurtosis, using a number of desired classes equal to 4.

For each cluster, the four-dimension centroid is computed. Each event is automatically assigned to the cluster having the nearest centroid.

The peak frequency of the assigned events has been plotted in time in order to understand the seasonal occurrence of each cluster. The grey rectangle indicates a period in which the station was tilted.

The results are shown in **Figure 16**.

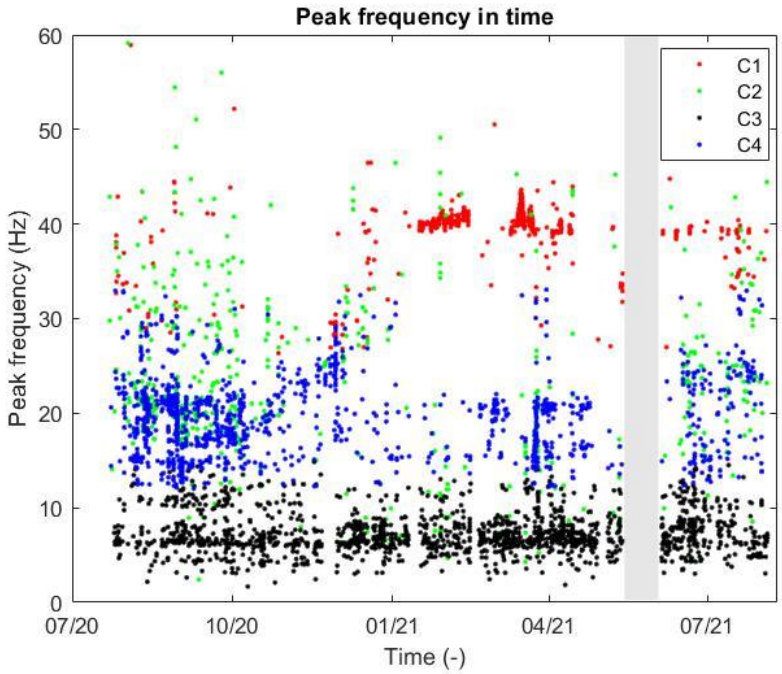

Figure 16. *Peak frequency in time of the four clusters (C1-C4) obtained using k-means algorithm on bracketed duration, kurtosis, peak frequency and 5 Hz frequency classes with the highest energy amount.*

The first cluster (*C1,* red in **Figure 16**) is mainly composed of events with frequencies around 40 Hz. The most events occur between January 2021 and May 2021, with only a few occurring during the remaining monitoring period, and in some cases, exhibiting lower frequencies. This may be a further indication that these events may be linked to snow compaction or melting.

The second cluster (*C2*, green in **Figure 16**) is characterized by events with strong frequency variability. Some events have low frequencies (around 10 Hz) while others reach up to approximately 50 Hz. Most events of this cluster take place in summer and autumn, even if some events do occur in other months, although infrequently.

The third cluster (*C3,* blue in **Figure 16**) contains events with frequencies ranging from approximately 10 Hz to 30 Hz, with the majority occurring between August and December. A small number of events occur in subsequent months. As a first

approximation, these events have been attributed to *high-frequency shallow quakes,* due to the fact that their frequency is variable over time and might be linked to shallow subsurface processes (e.g., icequakes in the active layer).

On the contrary, the last cluster (*C4*, black in **Figure 16**) does not display any seasonal variations. In fact, its events occur throughout the monitoring period and are always characterized by frequencies below or slightly above 10 Hz. Due to these characteristics, this cluster is probably representing *low-frequency deep quakes* and considering the visual classification, they may represent events correlated to the basal movements of the rock glacier.

To better understand the characteristics of the four clusters of events, a cross-plot of the peak frequency related to the bracketed duration has been computed, as shown in **Figure 17**.

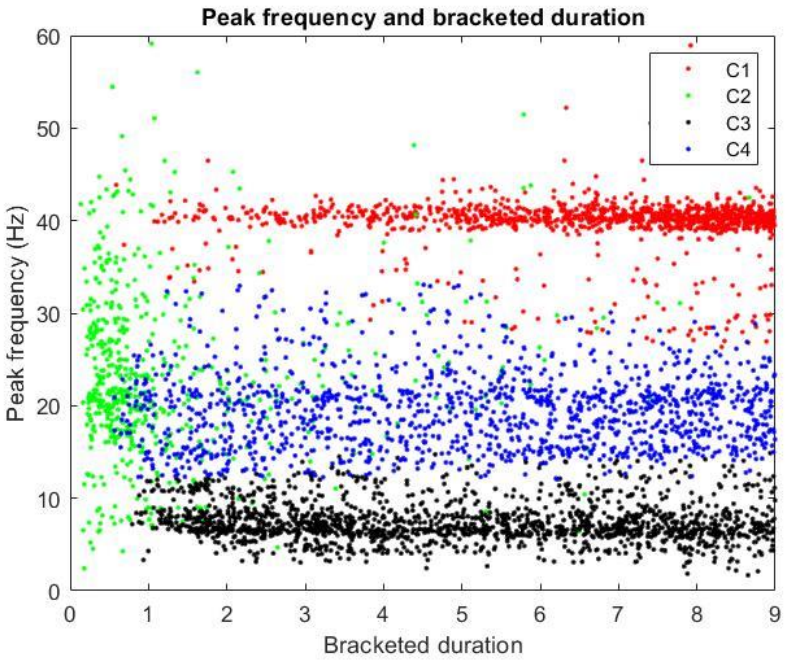

Figure 17. *Cross-plot of peak frequency vs bracketed duration of the four clusters (C1-C4).*

Looking at **Figure 17**, it is evident that events of clusters C1, C3 and C4 are characterized by comparable bracketed duration, ranging between 1 and 9 seconds.

On the contrary, most events of the second class (C2) exhibit considerably lower bracketed durations, typically within the range of 0 to 2 seconds. Though there exist several "outliers" with more extended durations, they are few.

Table 4. *Frequency and duration characteristics of the clusters C1 – C4.*

Cluster	Frequency (Hz)	Duration (s)
C1	40	1 – 9
C2	2 – 60	0 – 2
C3	≤ 10	1 – 9
C4	10 – 30	1 – 9

5.3.2 Relation with air temperature and precipitation data for 4 clusters analysis

The seasonal trend of the four classes obtained using k-means algorithm was then computed and compared to meteorological parameters of the site to get a more complete interpretation.

Air temperature and precipitation data are available from the meteorological station of ARPA Valle d'Aosta (Regional Agency for Environmental Protection) located close to the dam of the Goillet Lake, at 500-m distance from the rock glacier (https://presidi2.regione.vda.it/str_dataview_station/1700).

Hourly data are open access and can be downloaded from the web portal of the institution (https://presidi2.regione.vda.it/str_dataview_download).

The first step of the analysis was to perform the monthly occurrence of the events of each cluster and compare the result with monthly maximum, average and minimum temperature. This step would provide insights about the correlation between the temperature and the frequency of occurrence of each cluster.

For example, if a cluster occurs more frequently during summer when temperatures are higher, it could indicate that temperature plays a role in the behaviour of that cluster.

In a second moment, the events hourly occurrence of the month with the most events has been computed for each cluster (C1-C4) and compared to hourly maximum, average and minimum temperature.

The result for the cluster C1 is shown in the following graphs (**Figure 18** and **Figure 19**).

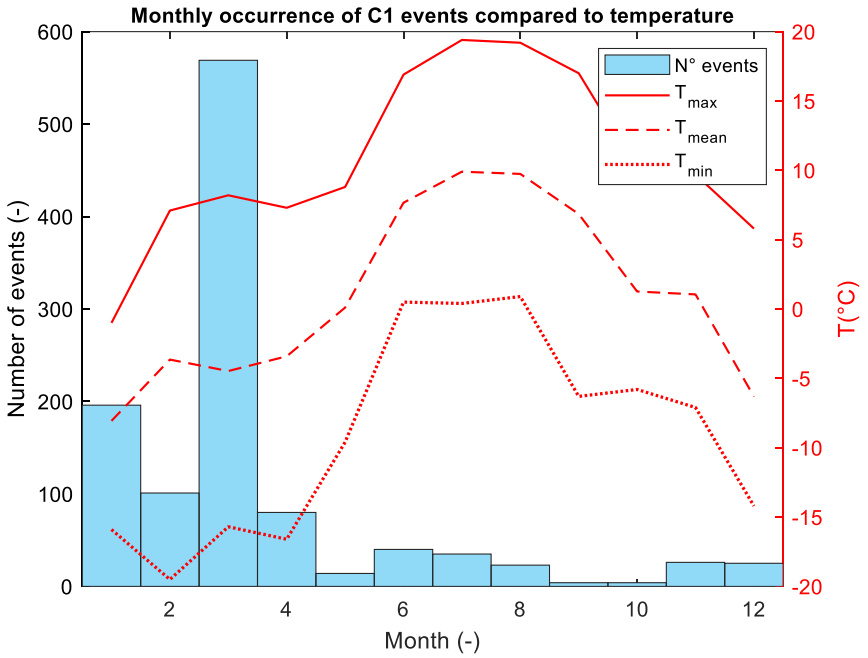

Figure 18. *Monthly occurrence of events of the first class (C1) compared to monthly maximum temperature (T_{max}), monthly average temperature (T_{mean}) and monthly minimum temperature (T_{min}).*

It is clear that the most events occur in March. In this month the maximum temperature registered is 8.2°C, the mean temperature is – 4.5 °C and the minimum temperature is – 15.7°C.

On the contrary, the months characterized by few events are the ones with highest temperature values. It is clear that this class of events is strongly related to colder periods.

Then, events of March have been investigated computing the hourly occurrence compared to hourly temperature values, as shown in figure **Figure 19**.

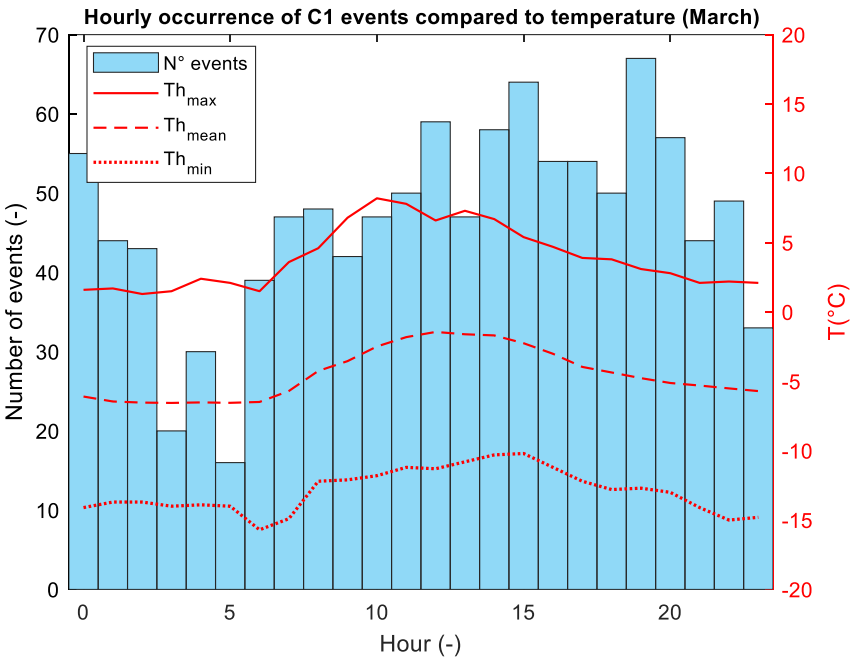

Figure 19. *Hourly occurrence of C1 events in March compared to hourly maximum temperature (Th_{max}), hourly average temperature (Th_{mean}) and hourly minimum temperature (Th_{min}).*

Looking at the figure above, the majority of C1 events occur in the afternoon, until midnight, then they decrease. Specifically, the highest incidence of events is at 7 p.m., whereas the lowest occurrence is observed during the time frame of 1 a.m. to 5 a.m.

The same analysis has been conducted on the C2 cluster and the outcomes are visible in **Figure 20**.

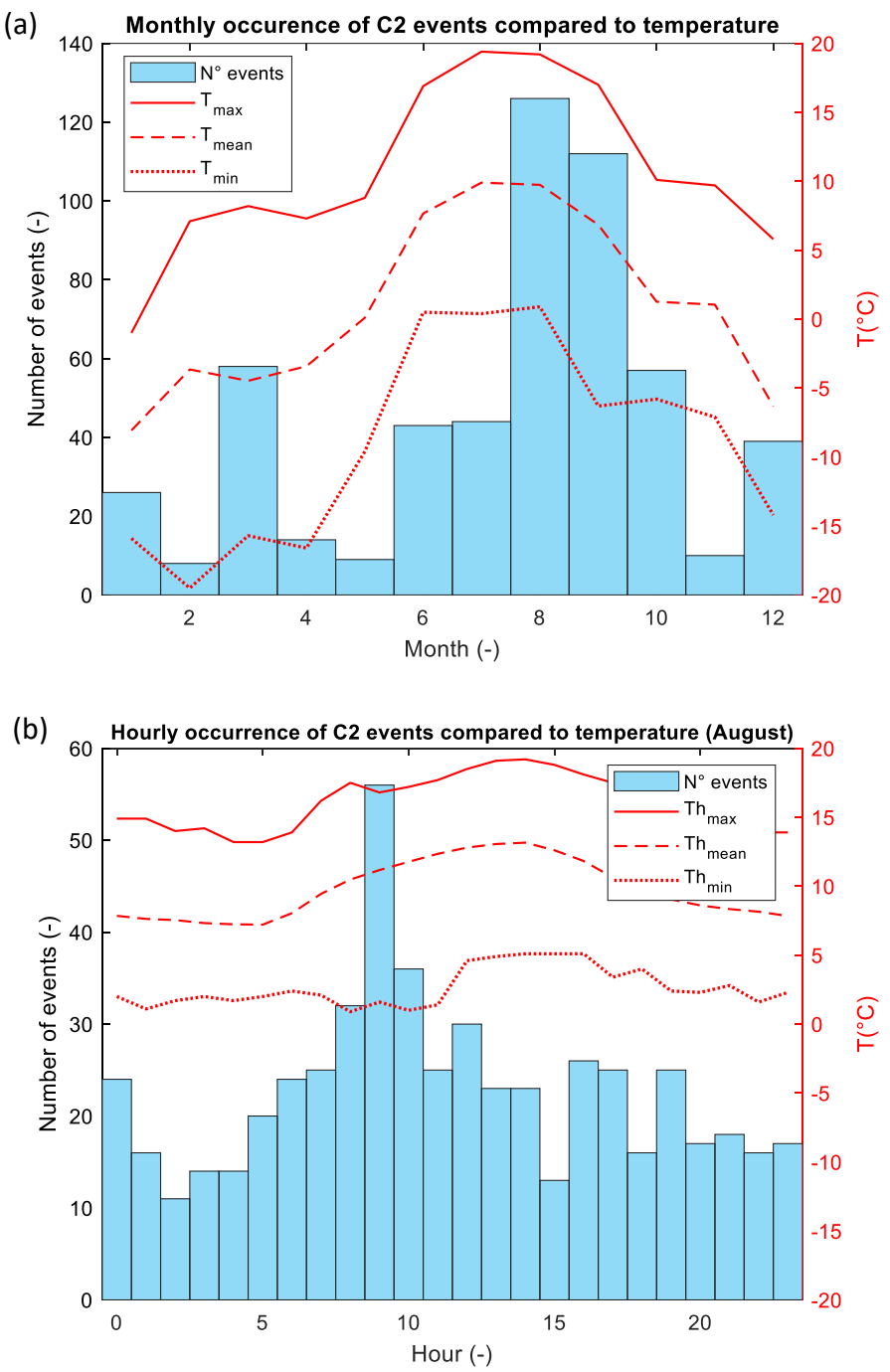

Figure 20. (a) *Monthly occurrence of events of the second class (C2) compared to monthly maximum temperature (T_{max}), monthly average temperature (T_{mean}) and monthly minimum temperature (T_{min}).* ***(b)*** *Hourly occurrence of C2 events in August compared to hourly maximum temperature (Th_{max}), hourly average temperature (Th_{mean}) and hourly minimum temperature (Th_{min}).*

Regarding the monthly occurrence of C2 events, they are strongly related to high temperature values. In fact, they mainly take place in August (126), when it is also reached the peak of temperature (Tmax = 19.2 °C, Tmean = 9.7 °C, Tmin = 0.9 °C).

However, the remaining events span all over the other months, but always with a number lower than 60.

Looking at the hourly occurrence of C2 events in August (**Figure 20b**), there is a strong peak of events at 9 a.m., when the maximum temperature is 16.8 °C, the mean temperature is approximately 11 °C and the minimum temperature is 1.6 °C. The lower incidence of events is in the afternoon and during night. For the cluster C3, the results of this analysis are visible in **Figure 21**.

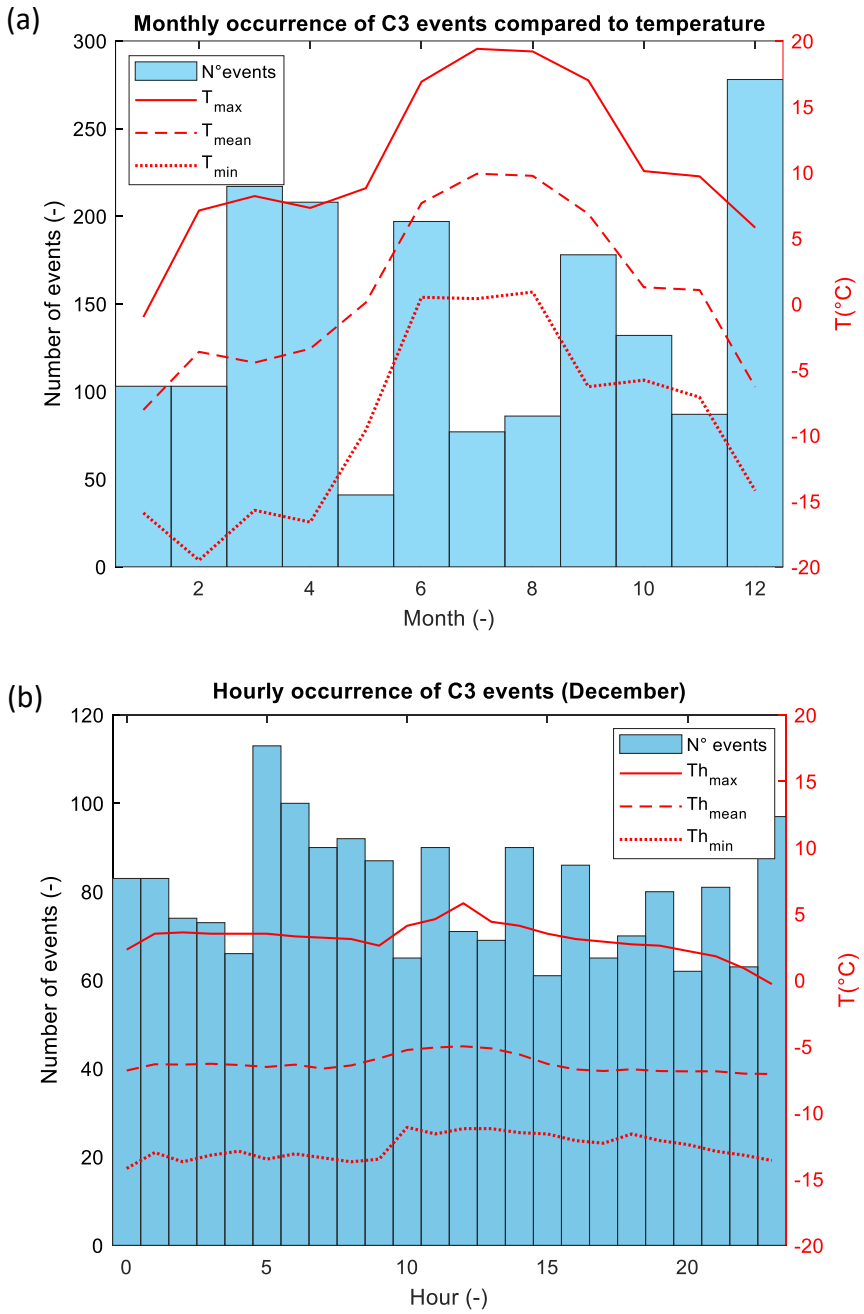

Figure 21. (a) *Monthly occurrence of events of the third class (C3) compared to monthly maximum temperature (T_{max}), monthly average temperature (T_{mean}) and monthly minimum temperature (T_{min}).* ***(b)*** *Hourly occurrence of C3 events in December compared to hourly maximum temperature (Th_{max}), hourly average temperature (Th_{mean}) and hourly minimum temperature (Th_{min}).*

The most of events of the third cluster take place in December (around 280), when the maximum temperature is 5.8 °C, the mean temperature is – 6.3 °C and the minimum temperature is -14.2 °C. The months with the low occurrence are instead July and August, corresponding to the warmer month, confirming that this class is related to colder periods. Looking at **Figure 21b**, it is possible to see that the hourly occurrence of these events is concentrated in the evening and during night (peak at 11 p.m.), while they decrease from 6 a.m. and 15 p.m.

Finally, the same analysis has been performed on the fourth cluster, as shown in **Figure 22**.

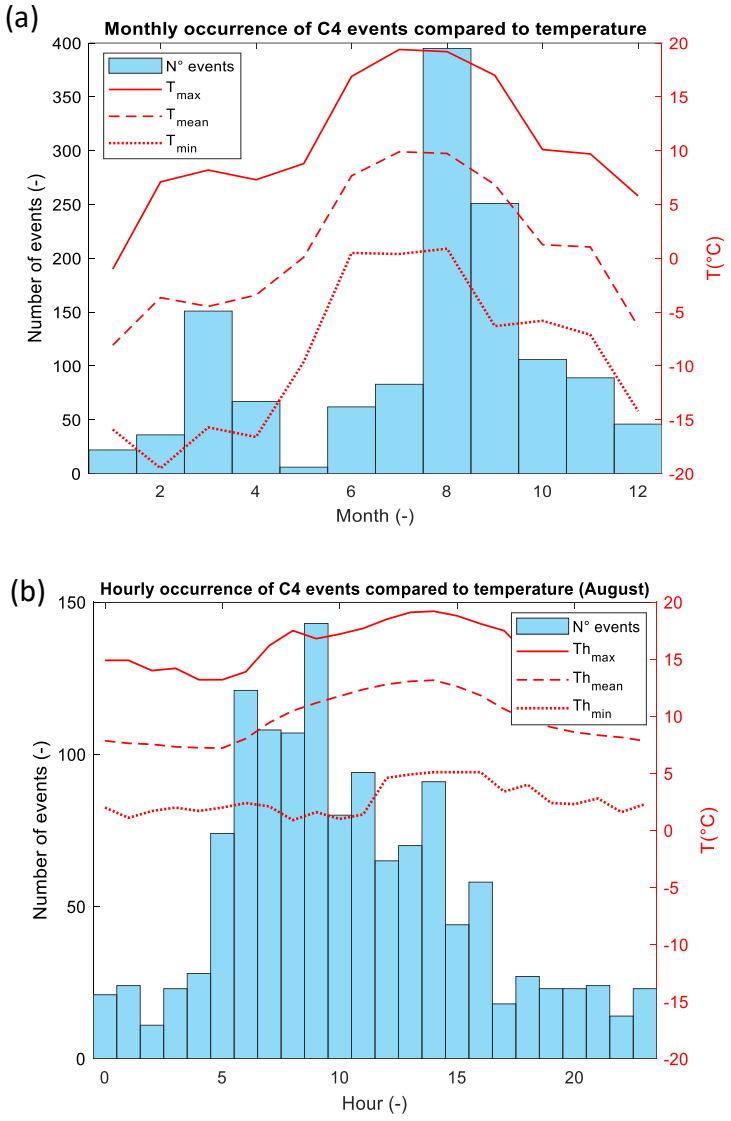

Figure 22. (a) *Monthly occurrence of events of the fourth class (C4) compared to monthly maximum temperature (T_{max}), monthly average temperature (T_{mean}) and monthly minimum temperature (T_{min}).* ***(b)*** *Hourly occurrence of C4 events in August compared to hourly maximum temperature (Th_{max}), hourly average temperature (Th_{mean}) and hourly minimum temperature (Th_{min}).*

The last cluster (C4) has the peak of occurrence in August, as for the second one (C2). Even the hourly occurrence is very similar because they both have most of the events in the early morning, reaching the peak at 9 a.m.

Table 5 shows a summary of the clusters' monthly and hourly occurrence previously described.

Table 5. *Monthly occurrence and hourly occurrence of the month with most events of the four clusters (C1-C4).*

Cluster	Highest occurrence month	Peak hour occurrence
C1	March	7 p.m.
C2	August	9 a.m.
C3	December	11 p.m.
C4	August	9 a.m.

5.3.3 K-means with 8 clusters

To better describe the dataset, the k-means algorithm was then applied on the same four parameters (peak frequency, bracketed duration, 5 Hz frequency classes containing the maximum energy amount and kurtosis) increasing the number of subclusters to 8. The objective is to better define the classes and to further analyse their characteristics as it may be necessary to use more than a single centroid to accurately define a class of events.

The peak frequency of the assigned events (C1 – C8) has been plotted in time to understand the seasonal occurrence of each cluster. The result is shown in **Figure 23**. The grey rectangle indicates a long period without data.

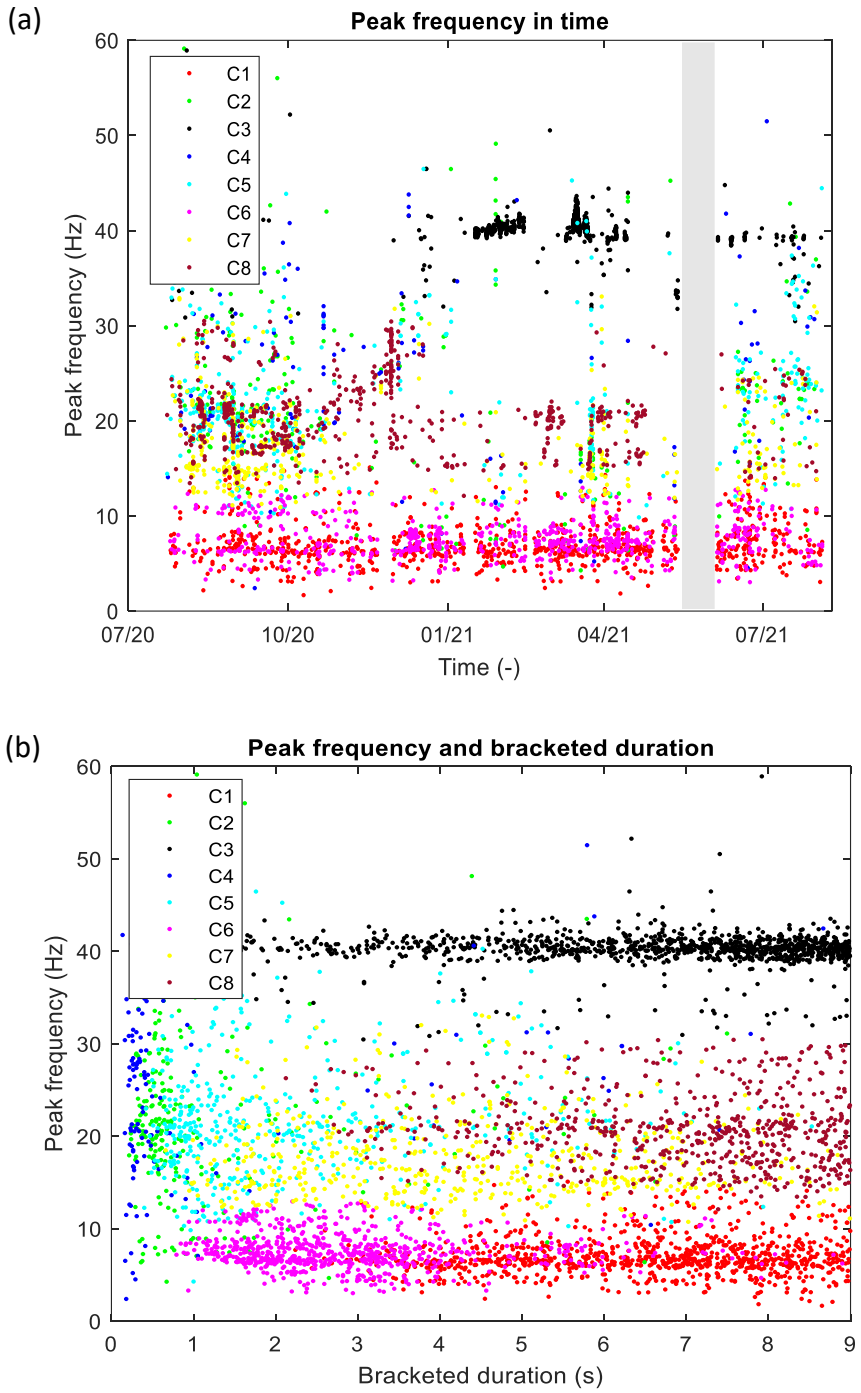

Figure 23. (a) *Peak frequency in time of the eight clusters (C1-C8) obtained using k-means algorithm on bracketed duration, kurtosis, peak frequency and 5 Hz frequency classes with the highest energy amount.* ***(b)*** *Peak frequency vs bracketed duration of the eight clusters (C1-C8).*

The red and magenta clusters (**C1** and **C6**) are characterized by events with frequencies that fall below or slightly above 10 Hz. The duration of events belonging to cluster C1 ranges from 1 to 5 seconds, whereas those in the sixth cluster (C6) last longer, typically between 4 and 9 seconds.

They are both registered throughout the monitoring period. It may be useful to compare them with climate data to identify further similarities in order to join them in a unique class.

The third cluster (**C3**, black) is analogous to the first class of the previous clustering attempt. Then, it is composed of events with frequency around 40 Hz and a bracketed duration of 1-9 seconds. These events occur predominantly from January 2021 to May 2021.

Clusters **C2** and **C4** (green and blue) are similar to each other with events that are the shortest in duration (below 1 second), exhibit strongly variable frequency, ranging from low values (around 2 Hz) to higher values (around 60 Hz). While many events in these clusters occur during autumn, outliers are observed in other months as well.

The fifth cluster (**C5**, cyan) contains events with frequencies ranging from approximately from 10 Hz to 40 Hz and short bracketed durations. These events primarily occur from August to December.

The yellow cluster (**C7**) is characterized by events with duration between 1 and 9 seconds and frequencies ranging from 10 Hz to 20 Hz. They are observed during the whole monitoring period but strongly decrease in winter.

Finally, eighth cluster (**C8**, bordeaux) is composed of events having frequencies that fall between 10 and 30 Hz. The bracketed duration of this class ranges from 3 s to 9 s but most of them lasts from 6 to 9 seconds.

In **Table 6** are shown the characteristics of the eight classes previously specified.

Table 6. *Frequency and duration range for the eight clusters obtained (C1-C8).*

Cluster	Frequency (Hz)	Duration (s)
C1	≤ 10	1 - 5
C2	2 - 60	≤ 1
C3	40	1 - 9
C4	2 - 60	≤ 1
C5	10 - 40	1 - 5
C6	≤ 10	1 - 5
C7	10 - 40	1 - 9
C8	10 - 30	3 - 9

Upon conducting a preliminary analysis of the results presented in the table above, similarities among the various classes have been observed.

Specifically, it appears that the first and sixth clusters could be combined, as could the C4 and C2 clusters.

Furthermore, the seventh and eighth classes exhibit comparable frequencies and durations, suggesting that they may be merged. Conversely, the C3 cluster stands out as a distinct class due to its unique frequency characteristics.

The remaining cluster (C5) may be comparable to C7 and C8 in terms of frequency, but the duration is different.

To better investigate the characteristics of these classes and the possibility to merge some of them, their seasonal trend is computed and compared to meteorological parameters. This analysis can provide insights into the factors that are driving the differences in frequency and duration of the eight clusters.

5.3.4 Relation with air temperature and precipitation data for 8 clusters analysis

The aim of this analysis is to explore similarities in the seasonal occurrence patterns of eight different classes (C1 – C8) and compare them to meteorological parameters, specifically temperature and precipitation data, recorded at the climate station of Goillet Lake.

As in the paragraph 5.3.2, the first analysis computed is the monthly occurrence for each cluster and the comparison to temperature data.

The second step involves identifying the month characterized by the most events for each class and then analysing the hourly occurrence of that month. This step would help to identify the specific time of the day when events' cluster is most likely to occur.

Overall, the aim of these analysis is to identify similarities in the seasonal occurrence patterns of the clusters and potentially merge some of them into a single class.

By merging clusters that have similar seasonal occurrence patterns, it may be possible to simplify the classification system and improve the understanding of the underlying meteorological and environmental factors that influence the formation

and behaviour of these clusters. The results for cluster C1 are shown in the following graphs (**Figure 24**).

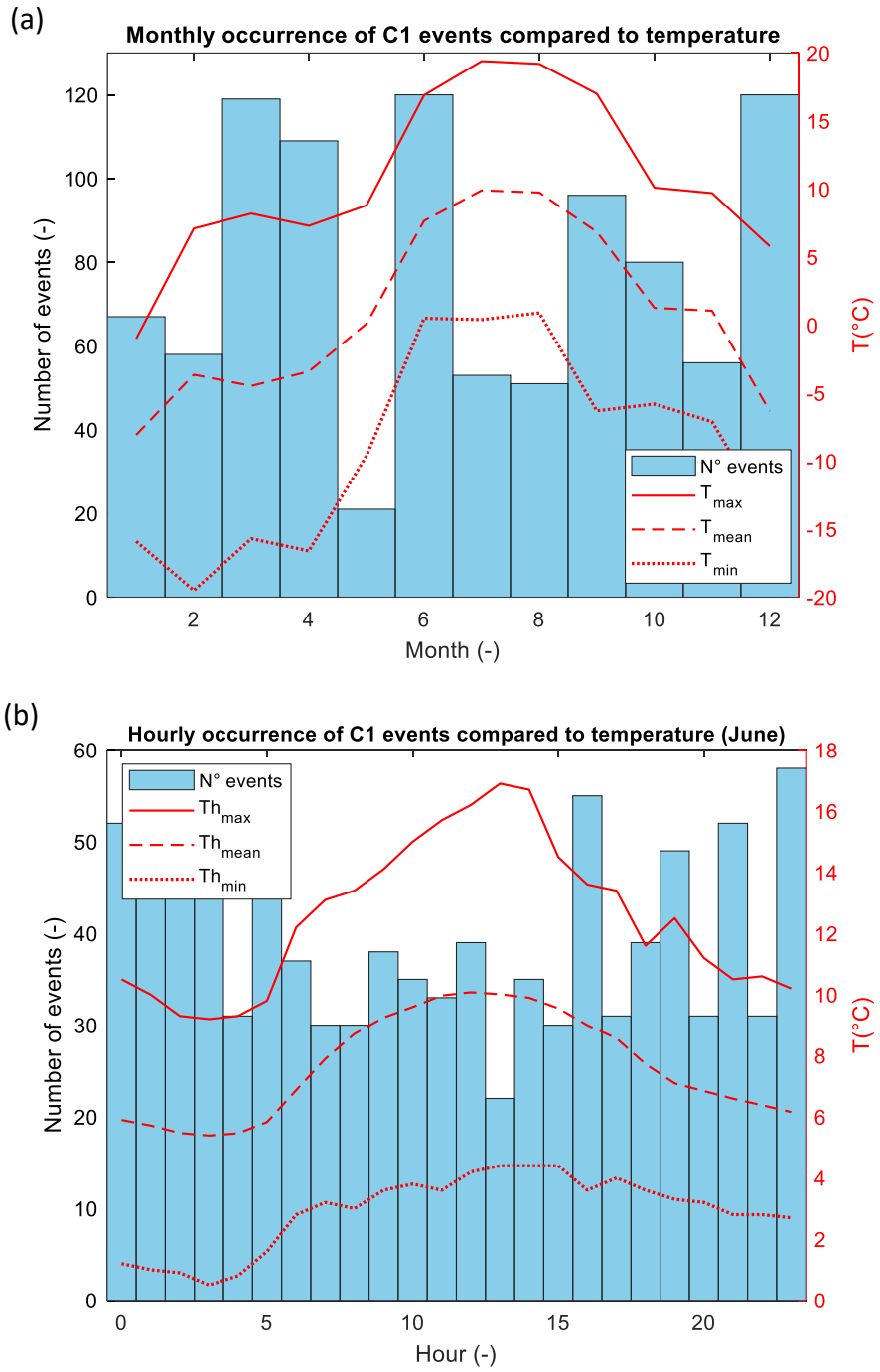

Figure 24. (a) *Monthly occurrence of events of the first class (C1) compared to monthly maximum temperature (T_{max}), monthly average temperature (T_{mean}) and monthly minimum temperature (T_{min}).* ***(b)*** *Hourly occurrence of C1 events in June compared to hourly maximum temperature (Th_{max}), hourly average temperature (Th_{mean}) and hourly minimum temperature (Th_{min}).*

The temporal distribution of cluster C1 (**Figure 24a**) shows a monthly pattern with multiple peaks of roughly 120 events occurring in March, June and December.

This pattern appears to be independent of temperature variations. Conversely, **Figure 24b** demonstrates an inverse relationship between cluster C1 and temperature. Specifically, during the hours of the day with the highest temperature (from 6 a.m. to 2 p.m.), the occurrence of events is observed to decrease.

The following image (**Figure 25**) shows the same analysis for the second cluster.

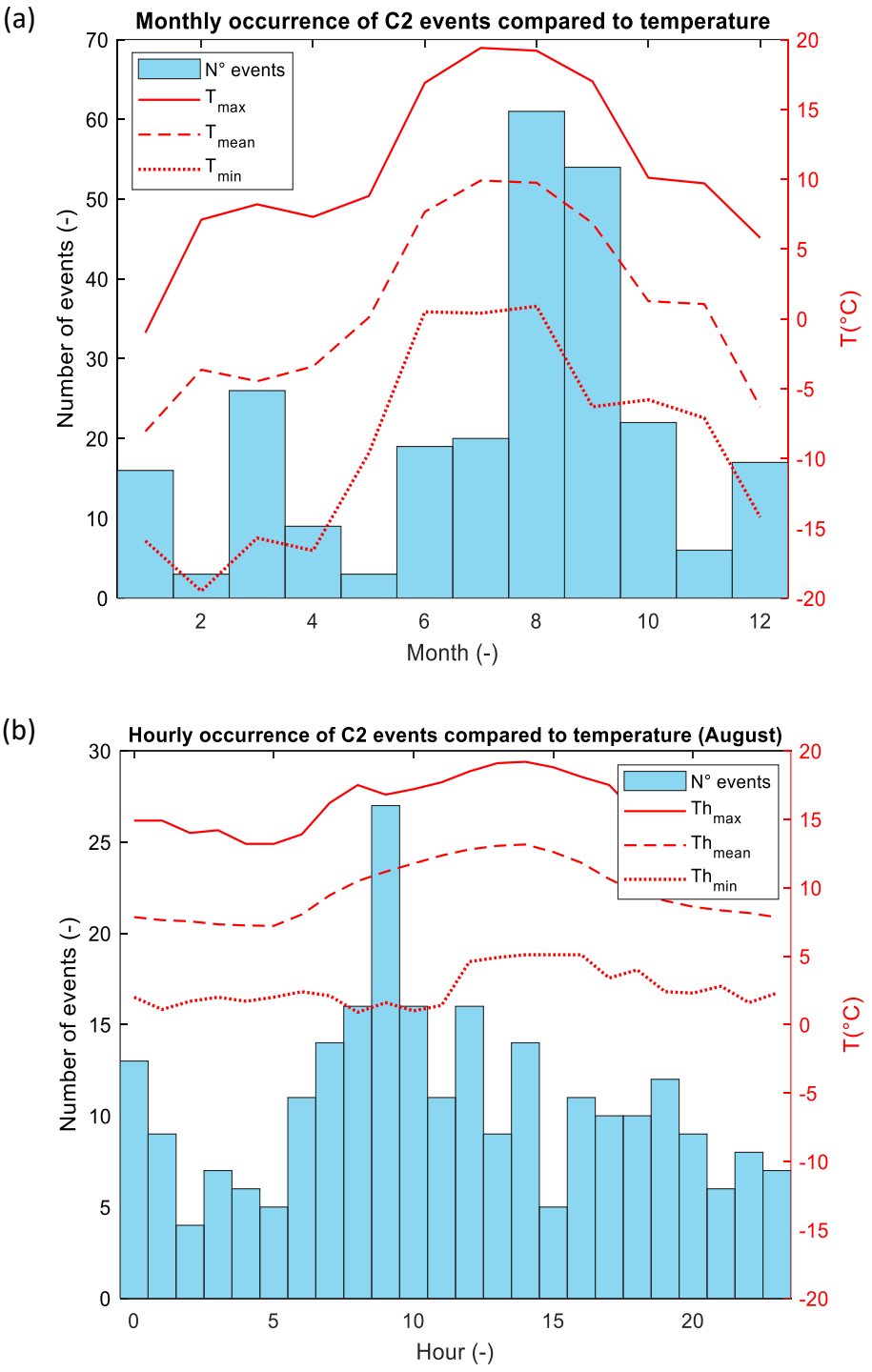

Figure 25. (a) *Monthly occurrence of events of the second class (C2) compared to monthly maximum temperature (T_{max}), monthly average temperature (T_{mean}) and monthly minimum temperature (T_{min}).* ***(b)*** *Hourly occurrence of C2 events in August compared to hourly maximum temperature (Th_{max}), hourly average temperature (Th_{mean}) and hourly minimum temperature (Th_{min}).*

The most events of the second class C2 take place in August and then in September.

It is possible that the high occurrence of cluster C2 in these months is related to the peak in temperature that occurs in July (monthly maximum temperature =19.4 °C,

monthly average temperature=10°C and monthly minimum temperature=0.4°C), as the effects of high temperatures may persist during the following months. The low occurrence of C2 events is in February, May, and November.

Looking at the hourly occurrence in August, it is visible that the peak of events happens in the morning, at 9 a.m.

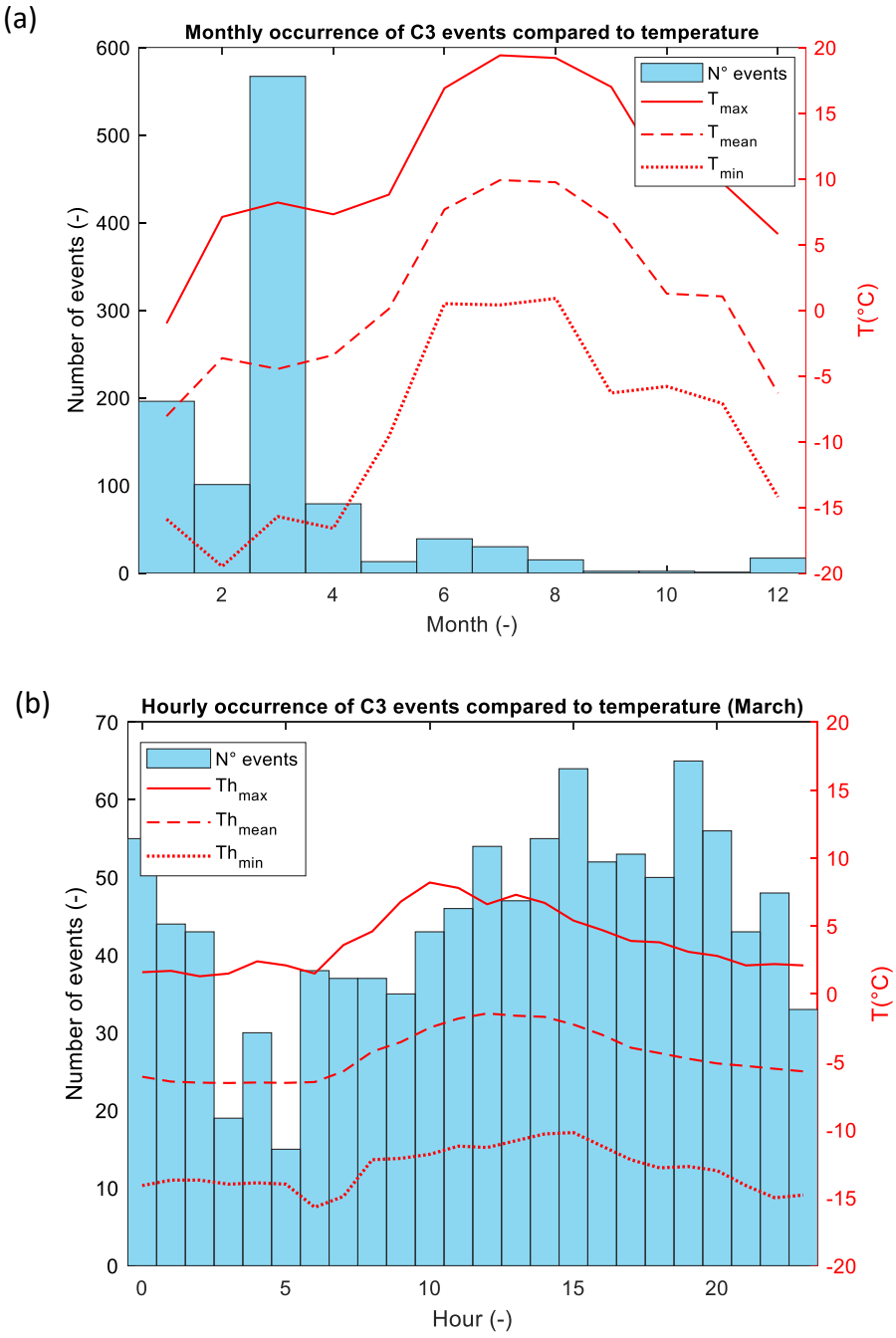

Figure 26. (a) *Monthly occurrence of events of the third class (C3) compared to monthly maximum temperature (T_{max}), monthly average temperature (T_{mean}) and monthly minimum temperature (T_{min}).* ***(b)*** *Hourly occurrence of C3 events in March compared to hourly maximum temperature (Th_{max}), hourly average temperature (Th_{mean}) and hourly minimum temperature (Th_{min}).*

The figures above (**Figure 26**) suggest that the third class (C3) is mainly characterized by events that occur in March, and the second month with the highest occurrence is January. This pattern may suggest that this class is related to colder periods, possibly related to snow compaction.

Furthermore, the fact that the majority of events in March occur in the afternoon and evening hours, with a peak at 7 p.m., when the temperature is low, suggests that this class may be related to specific atmospheric conditions that occur during those hours. For example, the cooling of the atmosphere as the sun sets may contribute to the conditions that lead to C3 events.

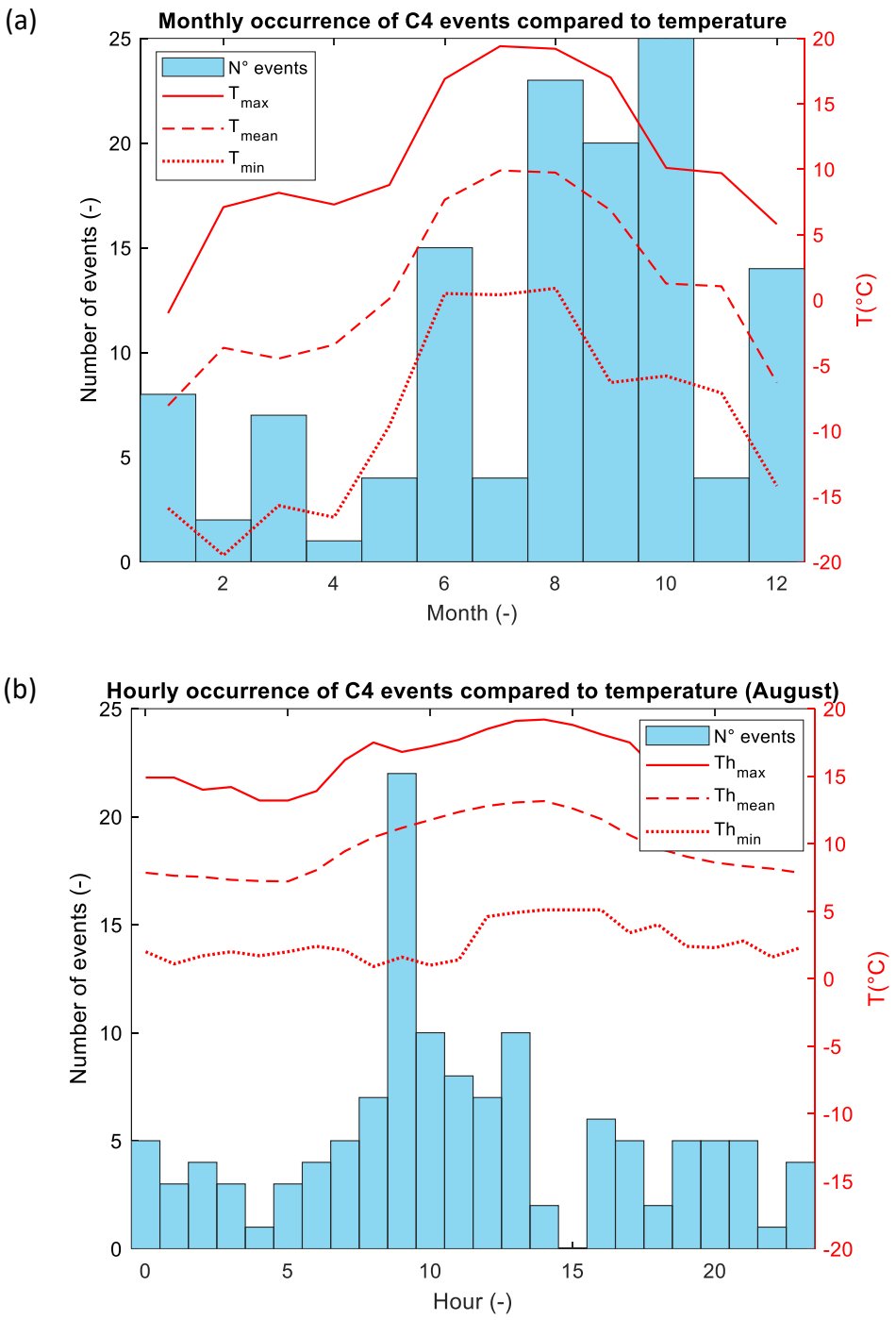

Figure 27. (a) *Monthly occurrence of events of the fourth class (C4) compared to monthly maximum temperature (T_{max}), monthly average temperature (T_{mean}) and monthly minimum temperature (T_{min}).* ***(b)*** *Hourly occurrence of C4 events in August compared to hourly maximum temperature (Th_{max}), hourly average temperature (Th_{mean}) and hourly minimum temperature (Th_{min}).*

The fourth category of events (C4) predominantly occurs in October with 25 events registered (**Figure 27a**). Nevertheless, high occurrences of this event type are also observed in August and September. It appears that the prevalence of C4 events is

correlated to periods of elevated temperature, as the number of occurrences decreases in other months, even though by a marginal amount.

Regarding the hourly occurrence in August, the peak occurs at 9 a.m, with 22 events registered and a maximum temperature of 16.8 °C, a mean temperature of 11.1 °C and and a minimum temperature of 1.6 °C.

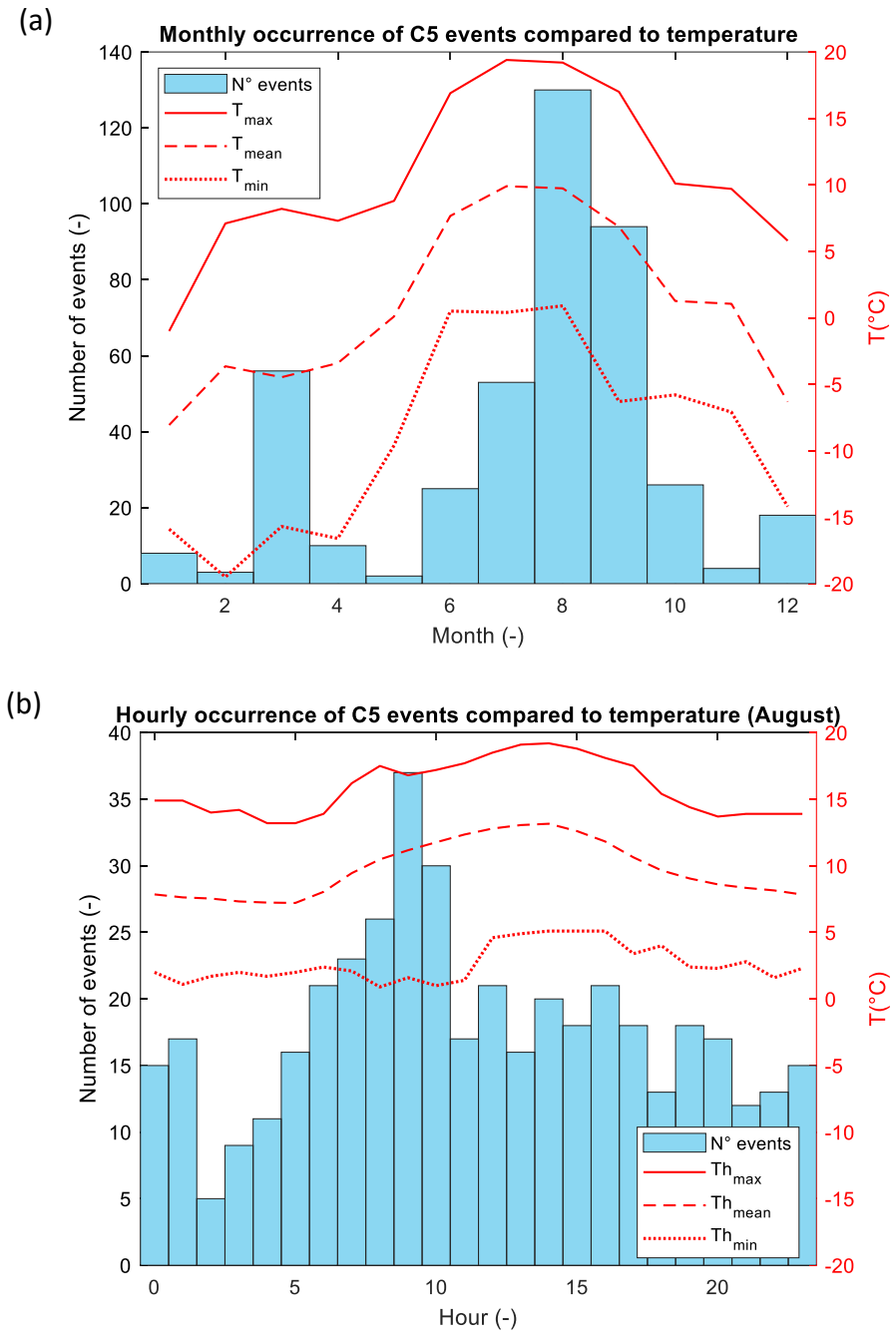

Figure 28. (a) *Monthly occurrence of events of the fifth class (C5) compared to monthly maximum temperature (T_{max}), monthly average temperature (T_{mean}) and monthly minimum temperature (T_{min}).* ***(b)*** *Hourly occurrence of C5 events in August compared to hourly maximum temperature (Th_{max}), hourly average temperature (Th_{mean}) and hourly minimum temperature (Th_{min}).*

In the fifth cluster (C5) a total of 429 events were observed, with the majority taking place during the month of August (130) when the highest recorded temperature was 19.2 °C (**Figure 28**). The second most frequent month for these events was September, with a total of 94 occurrences. On the contrary, the remaining months of the year registered a low number of events (below 60).

In August, the peak of events (37) occurs at 9 a.m when the maximum temperature was 16.8 °C and the lowest temperature is 1.6 °C.

It is not the warmer hour of the day, but it is clear that the most events take place in the morning.

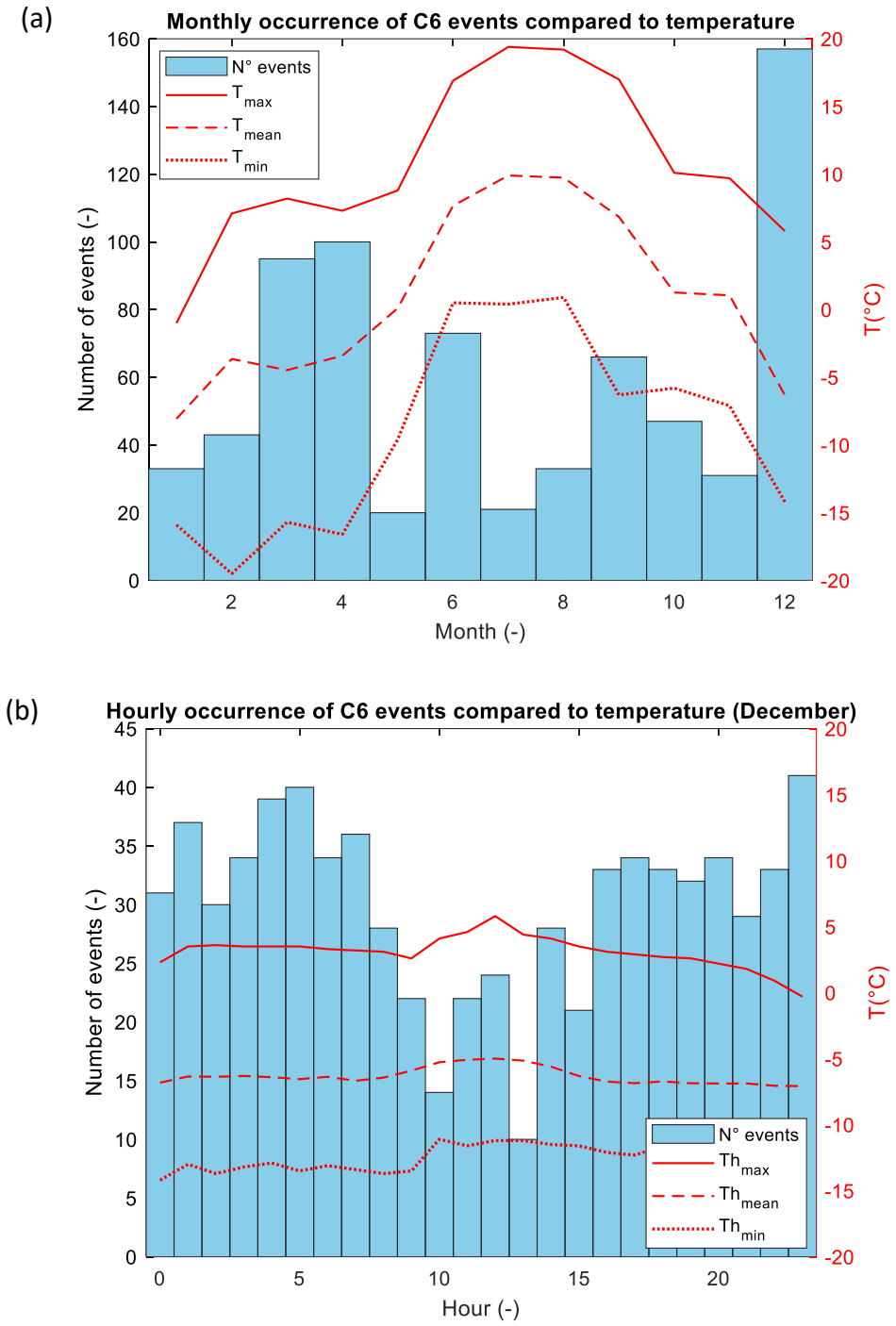

Figure 29. (a) *Monthly occurrence of events of the sixth class (C6) compared to monthly maximum temperature (T_{max}), monthly average temperature (T_{mean}) and monthly minimum temperature (T_{min}).* ***(b)*** *Hourly occurrence of C6 events in December compared to hourly maximum temperature (Th_{max}), hourly average temperature (Th_{mean}) and hourly minimum temperature (Th_{min}).*

The cluster C6 is characterized by events that mainly occur in December (157), as shown in **Figure 29**. The other two months with highest occurrence are March and April, with 95 and 100 events, respectively.

In December, there is no evident peak of events during any particular hour of the day. However, the majority of events take place between 11 p.m. and 5 a.m. when air temperature is low.

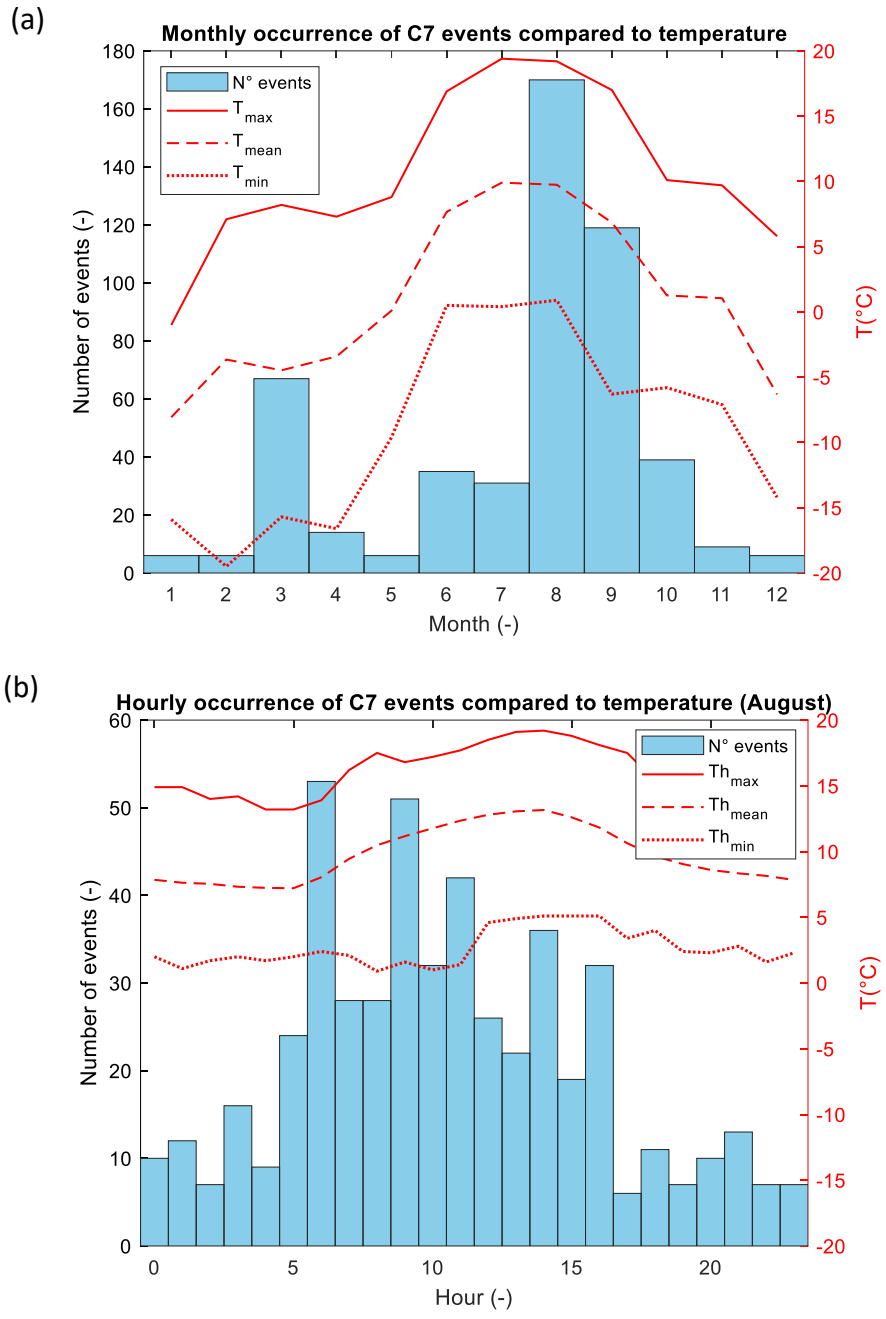

Figure 30. (a) *Monthly occurrence of events of seventh class (C7) compared to monthly maximum temperature (T_{max}), monthly average temperature (T_{mean}) and monthly minimum temperature (T_{min}).* ***(b)*** *Hourly occurrence of C7 events in August compared to hourly maximum temperature (Th_{max}), hourly average temperature (Th_{mean}) and hourly minimum temperature (Th_{min}).*

The monthly occurrence of cluster C7 is characterized by a strong peak of events in August (170) followed by a subsequent peak in September (119). These occurrences are correlated with elevated temperatures observed during this period, whereby the maximum temperature (T_{max}) averages at 19.2 °C, the mean temperature (T_{mean}) is 9.7 °C and the minimum temperature (T_{min}) is 0.9 °C.

In August, the time range featuring the highest incidence of cluster C7 events is from 6 a.m. to 2 p.m., corresponding with the period of the day in which temperatures are highest (**Figure 30**).

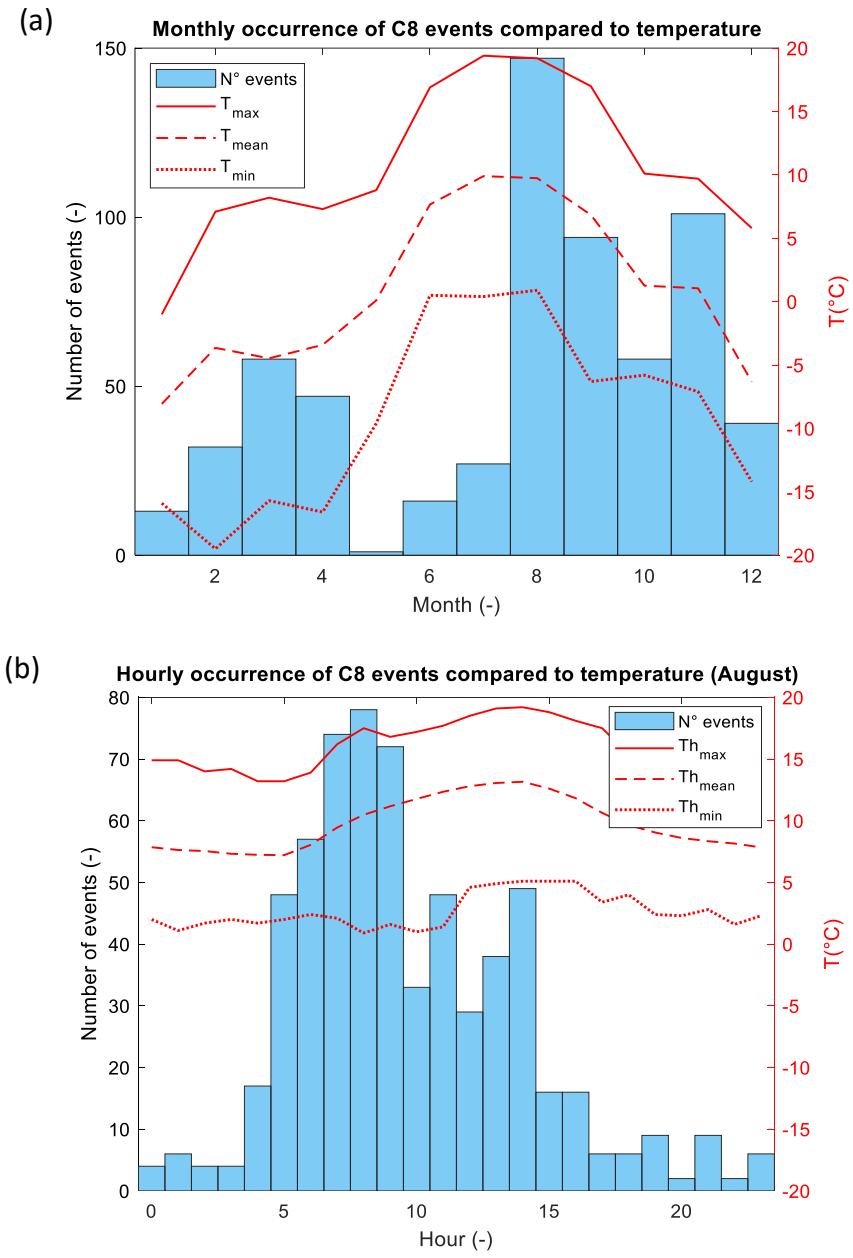

Figure 31. (a) *Monthly occurrence of events of eighth class (C8) compared to monthly maximum temperature (T_{max}), monthly average temperature (T_{mean}) and monthly minimum temperature (T_{min}).* ***(b)*** *Hourly occurrence of C8 events in August compared to hourly maximum temperature (Th_{max}), hourly average temperature (Th_{mean}) and hourly minimum temperature (Th_{min}).*

Regarding the final class of events (C8), August stands out as the month with the highest number of registered occurrences, with a total of 147. The second month with highest incidence is November, with 101 events recorded (**Figure 31**).

Furthermore, the majority of events within this cluster take place in the morning, specifically between 5 a.m. to 9 a.m., with a peak incidence at 8 a.m. Subsequently, the frequency of recorded events gradually decreases throughout the day, with very few events occurring during the afternoon hours.

The **Table 7** summarises the occurrence characteristics of each cluster previously specified.

Table 7. *Month with highest events' occurrence and hourly occurrence peak during that month of each cluster (C1-C8).*

Cluster	Highest occurrence month	Peak hour occurrence
C1	June	11 p.m.
C2	August	9 a.m.
C3	March	7 p.m.
C4	October	9 a.m.
C5	August	9 a.m.
C6	December	11 p.m.
C7	August	6 a.m.
C8	August	8 a.m.

In addition, the occurrence cumulative curves of the eight classes (C1-C8) have been plotted in time and compared to meteorological data, such as temperature (T°C), precipitation (mm/h) and snowfall (cm) registered at the reference meteorological station during the monitoring period.

The occurrence cumulative curves of the different classes give us information about the periods with most events. When the curve for a particular class is steep, it indicates a high occurrence of events during that period, while a flat curve indicates a low occurrence. The result is visible in **Figure 32**.

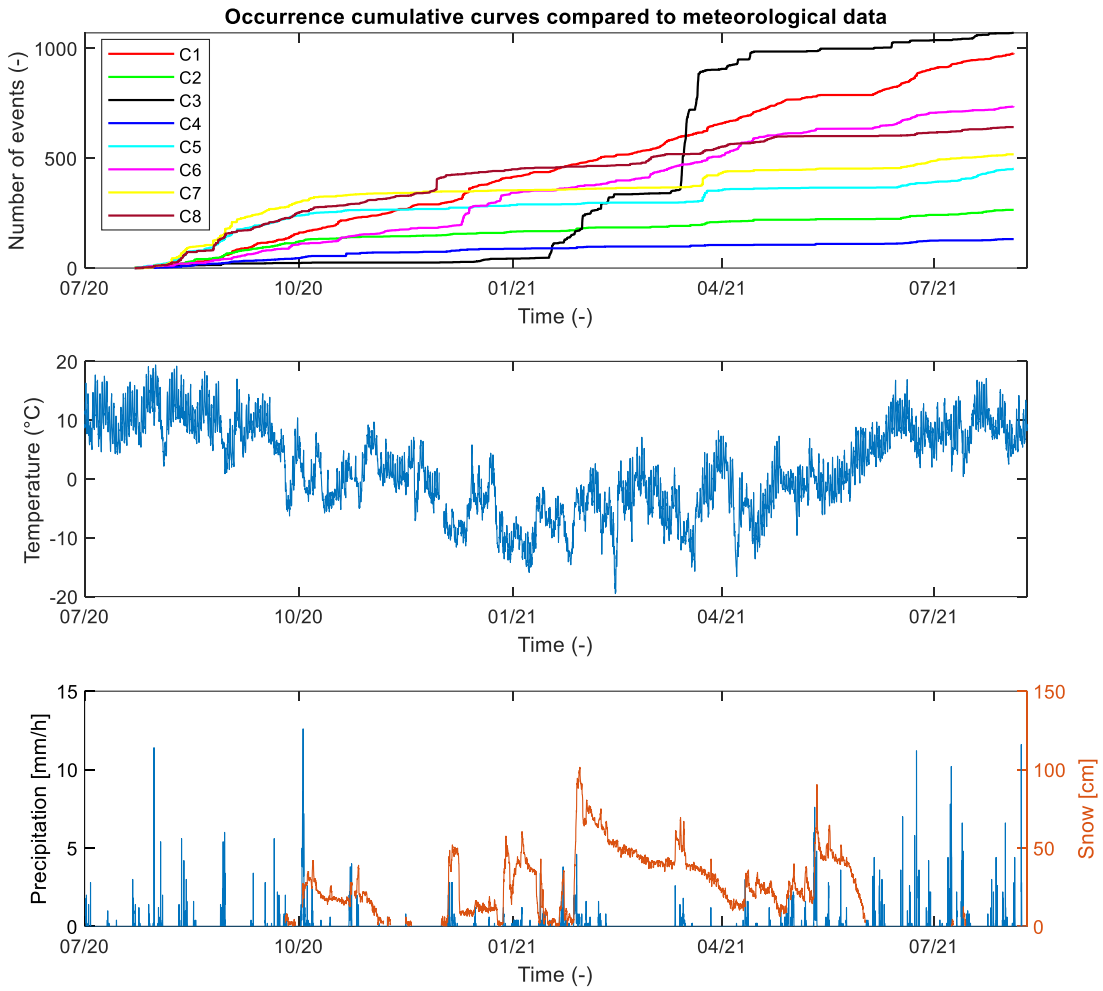

Figure 32. *Occurrence cumulative curves of the eight clusters (C1-C8) and temperature (°C), precipitation (mm/h) and snowfall (cm) registered during the monitoring period.*

Taking into account the similarities observed among the eight clusters (C1 – C8) in terms of seasonal incidence and correlation with temperature data and the cumulative curves of occurrence, it may be advisable to merge certain classes.

In particular, the clusters C7 and C8 exhibit similar peak frequency ranges and durations (**Table 6**). In addition, both clusters display a peak of events in August, concomitant with high temperatures (**Table 7**). Moreover, these events occur during the hours of the day when temperatures begin to rise (morning). For these reasons they are probably related to variations of the active layers of the rock glaciers that may lead to icequakes and other fracturing processes. They are finally classified as “high-frequency shallow quakes”.

Other two classes that may be merged are C1 and C6, given their occurrence during colder months. Although C1 exhibits two notable peaks in March and June, both clusters are characterized by nocturnal events that coincide with lower temperatures. These events may be linked to basal movements of the rock glaciers, as well as rock and debris slides on the rock glaciers and in the surroundings. The events captured by the peak in June of cluster C1 are likely attributable to rock falls, while events of cluster C6 are predominantly deeper quakes. Differentiating between quakes and rock falls based on the clustering analysis parameters is challenging. However, these classes are merged and classified as “low-frequency deep quakes”.

On the contrary, the third cluster of events (C3) represents a unique class. They are related to snow compaction or melting that lead to stress variation within the rock glaciers, as confirmed also by the steep period of the occurrence cumulative curve in **Figure 32**. These events occur during periods of snow cover, with a peak incidence in March, occurring later than the peak of air temperature. The delay may be attributed to the time required for thermal propagation within the snow and the rock glaciers.

The remaining clusters C2, C4 and C5 are characterised by similar histograms but they are further investigated in relation to rainfall to assess the feasibility of merging them.

More precisely, the monthly occurrence of the three classes (C2, C4 and C5) has been computed and compared to the monthly maximum precipitation (P_{max}) and to the monthly mean precipitation (P_{mean}). In addition, the hourly occurrence in the month with highest number of events of the three clusters has been compared to the hourly maximum precipitation (Ph_{max}) and to the hourly mean precipitation (Ph_{min}).

The following figure shows the results for the cluster C2.

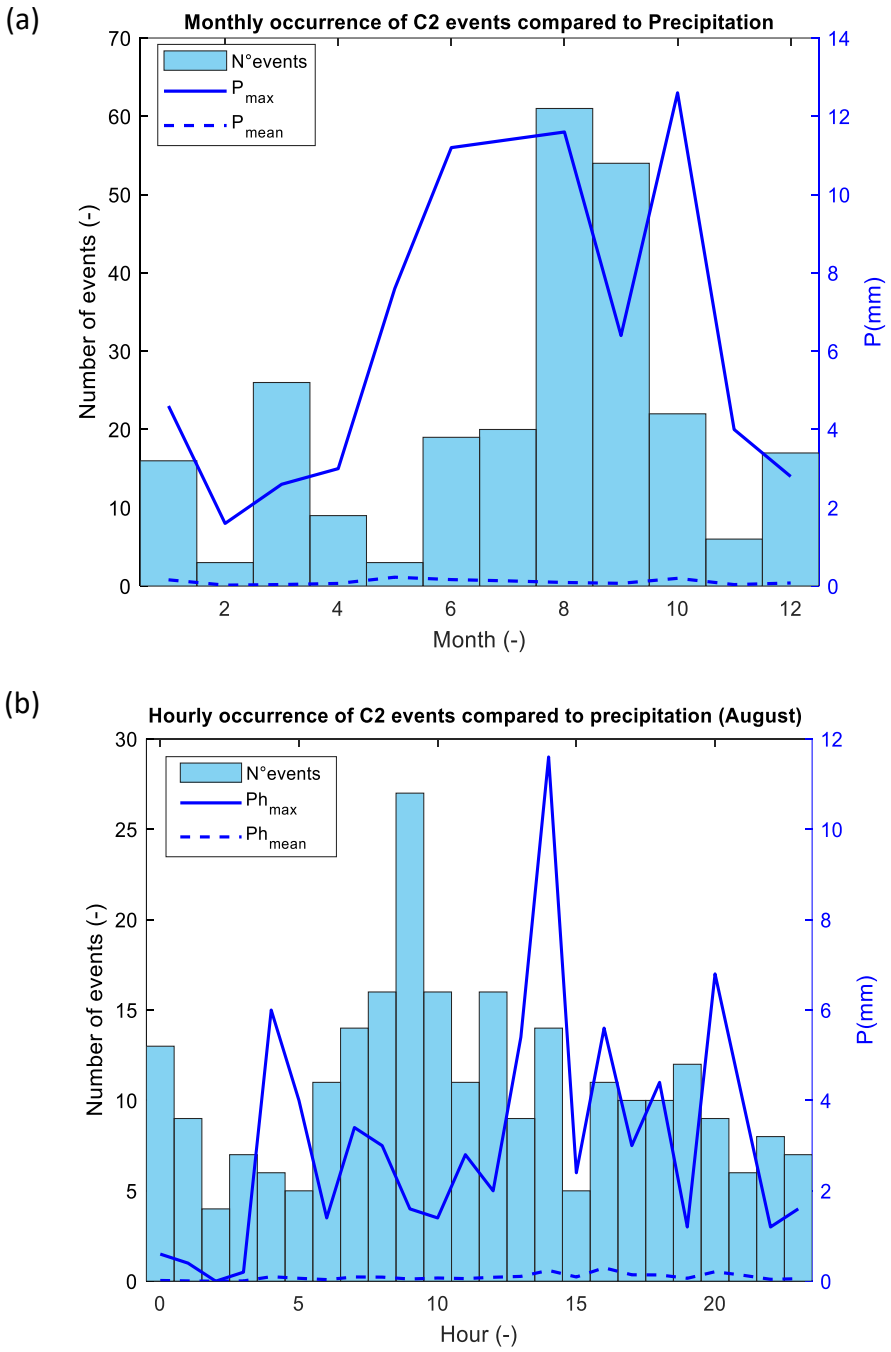

Figure 33. (a) *Monthly occurrence of events of the second class (C2) compared to monthly maximum precipitation (P_{max}) and monthly average precipitation (P_{mean}).* ***(b)*** *Hourly occurrence of C2 events in August compared to hourly maximum precipitation (Ph_{max}) and hourly average precipitation (Ph_{mean}).*

Figure 33a shows that the peak of 61 events occurs in August, concurrently with a peak in the monthly maximum precipitation (11.6 mm), even if the hourly occurrence during August does not indicate any correlation with rainfall events. It is only visible that there are always events during rainfall.

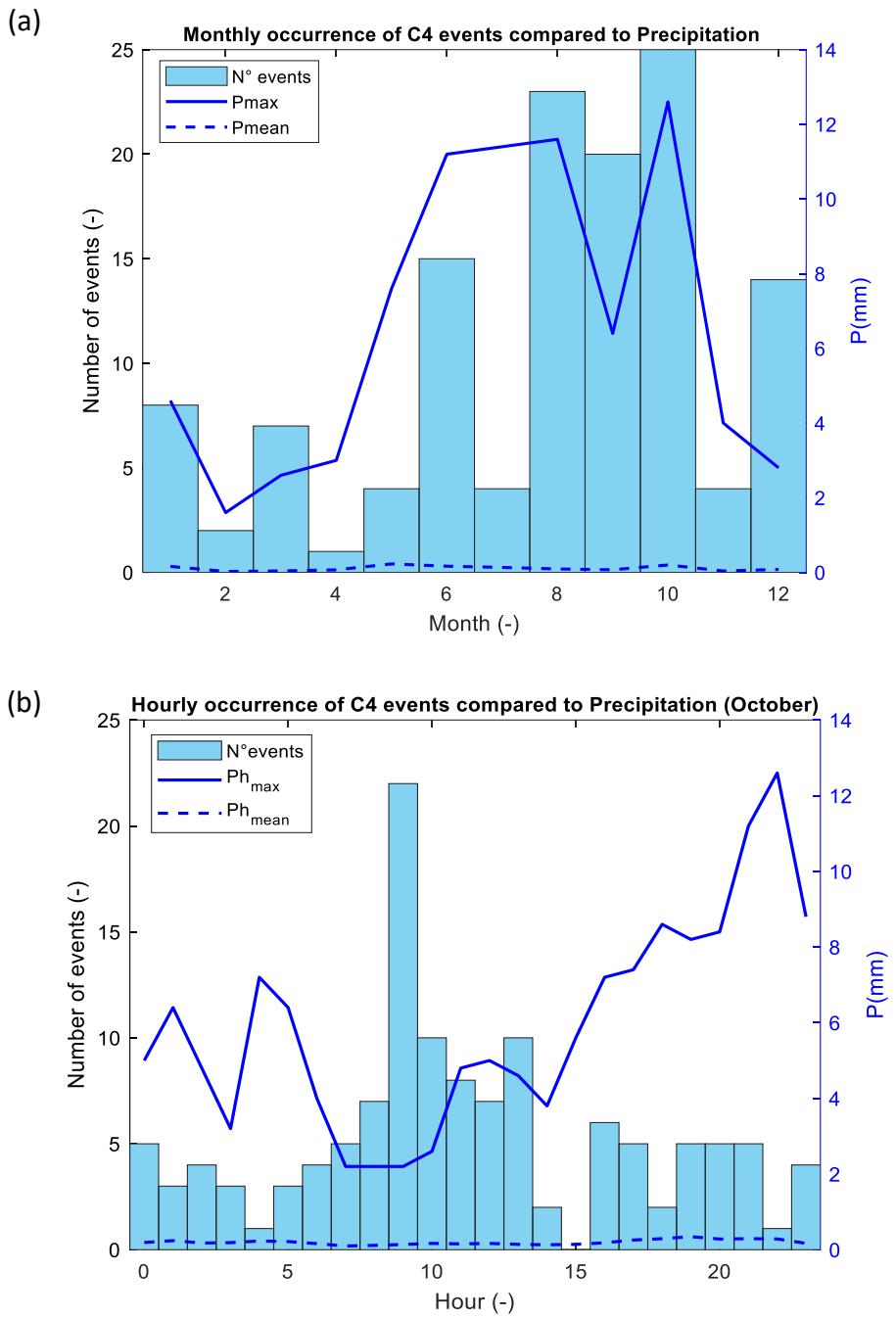

Figure 34. (a) *Monthly occurrence of events of the fourth class (C4) compared to monthly maximum precipitation (P_{max}) and monthly average precipitation (P_{mean}).* ***(b)*** *Hourly occurrence of C4 events in October compared to hourly maximum precipitation (Ph_{max}) and hourly average precipitation (Ph_{mean}).*

The C4 class is characterized by a peak of events in October, as visible in **Figure 34a**. This month is the one with the highest level of precipitation with August following closely behind, recording 12.6 and 11.6 mm, respectively. Thus, it appears to be a significant correlation between these events and rainfall patterns. **Figure 34b**, on the other hand, does not demonstrate this correlation as explicitly.

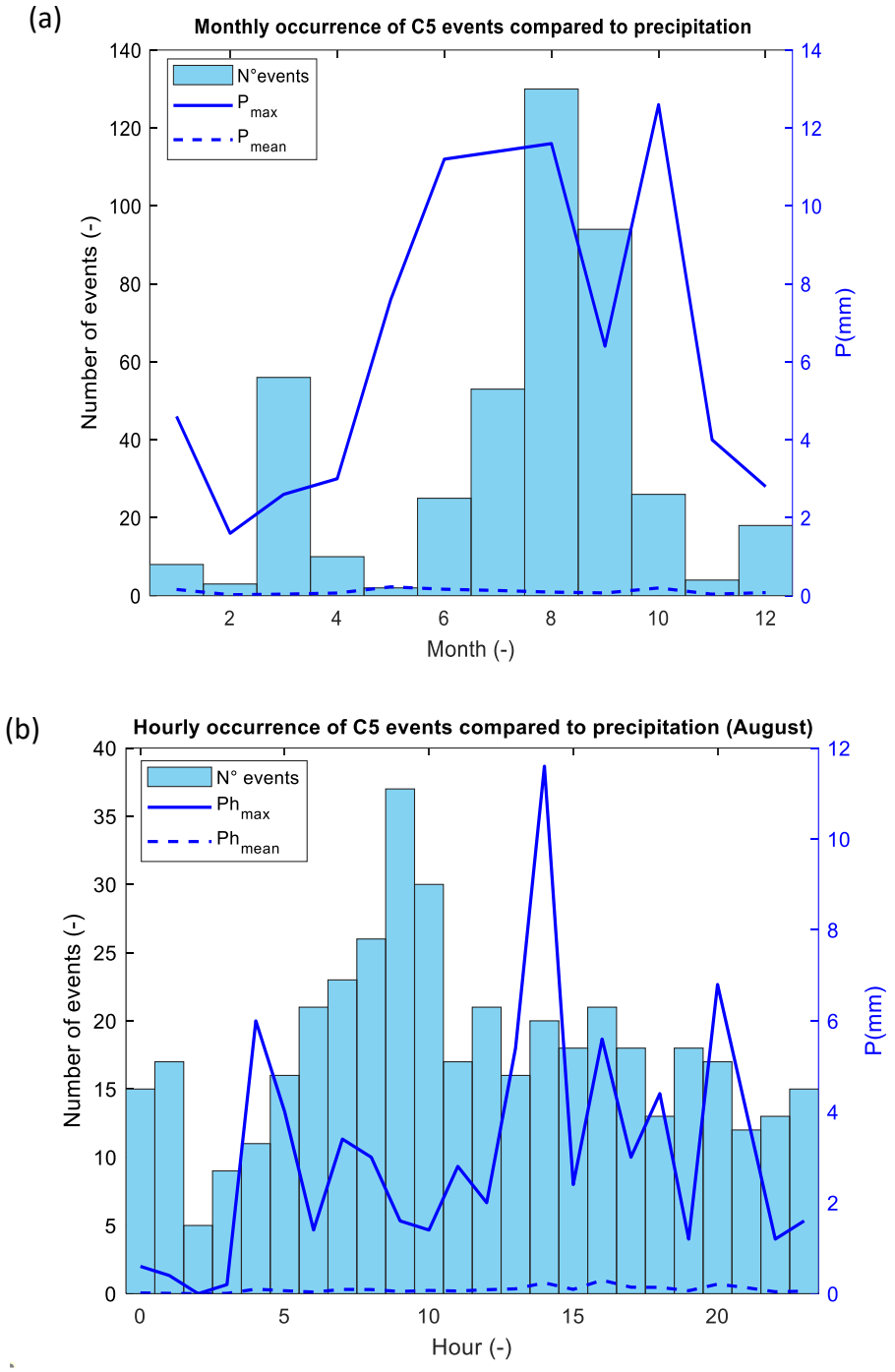

Figure 35. *Monthly occurrence of events of the fifth class (C5) compared to monthly maximum precipitation (P_{max}) and monthly average precipitation (P_{mean}).* ***(b)*** *Hourly occurrence of C5 events in August compared to hourly maximum precipitation (Ph_{max}) and hourly average precipitation (Ph_{mean}).*

Even the fifth class (C5) is characterized by a peak of 130 events in August, when the precipitation registered is 11.6 mm, as shown in **Figure 35a**.

As for the other classes (C2 and C4), the hourly occurrence in August does not explicitly indicate this correlation.

Subsequently, to better understand the correlation of the three classes (C2, C4 and C5) with rainfall patterns, the percentage of clusters events occurred during precipitations events has been computed. The outcomes are shown in **Table 8**.

Table 8. *Percentage of events occurring during rainfall for clusters C2, C4 and C5.*

Cluster	Events (%)
C2	21.6
C4	22.2
C5	16.2

Looking at the table above, it is possible to see that the percentage of events that occur during precipitation, even if low, is not negligible.

Finally, these three clusters have been merged in a singular class mainly composed by “rainfall-related events” even though including high-frequency short duration events as well.

As a final analysis, the comparison between the cumulative curves resulting from the clustering with four classes and those of the clustering with 8 sub-classes is computed. The result is shown in **Figure 36.**

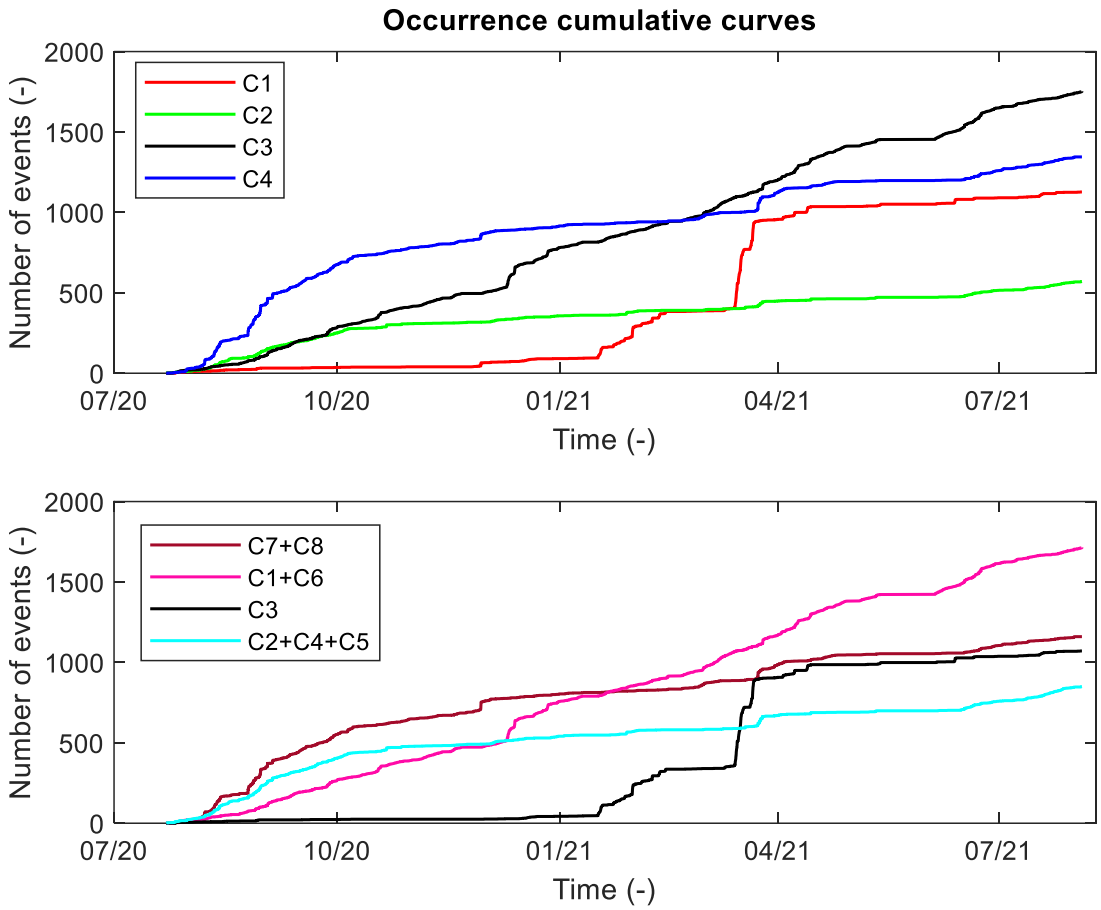

Figure 36. *Comparison between the occurrence cumulative curves of clustering with 4 classes and 8 classes.*

It is clear that there are no substantial differences between the cumulative curves of the two cluster analyses. In particular, clusters C1 (4 classes) and C3 (8 classes) show an identical trend. The same is for the comparison between clusters C3 (4 classes) and C7+C8 (8 classes). Clusters C4 (4 classes) and C7+C8 (8 classes) show similar trends, but a slightly different number of events. The main differences occur between the combined class C2+C4+C5 (8 classes), in comparison with cluster C2 (4 classes). The first clustering attempt had a small number of occurrences within this class (C2) with respect to the second attempt(C2+C4+C5).

Such observations may imply that in the first case, some events were allocated to other classes, indicating a potential for errors or misclassifications.

Therefore, increasing the number of sub-clusters may enhance the clustering algorithm's ability to assign each event to its appropriate class, avoiding outliers and inaccuracies.

In any case, the coherence of the two clustering results highlights the robustness of the selected clustering parameters to obtain a fast and reliable automatic classification of the detected events.

6 CONCLUSIONS

As previously discussed, the objective of this thesis was to perform a seismic survey to investigate the dynamics and internal processes of Gran Sometta rock glaciers. To achieve this, the analysis of the seismic dataset obtained through the installation of four monitoring stations (GEA2-GEA5) has revealed the existence of a significant number of microseismic events throughout the monitoring period, as indicated in the Section 5.1.

Specifically, the application of the short-time average over the long-time average (STA/LTA) algorithm to the raw signals resulted in the extraction of 45326 total events, which were differentially distributed among the four seismic stations (Table 3).

The events identified at the GEA2 station were subjected to a process of classification through both visual analysis and cluster analysis based on kurtosis, bracketed duration, 5-Hz frequency classes containing the highest energy amount and peak frequency of the amplitude spectrum.

The visual (manual) classification conducted analysing the seismogram, Fourier spectrum and spectrogram, yielded six distinct types of events, namely: low frequency and long duration events, earthquakes, rockfalls, rain-related noise events, snow-related events and high frequency and short duration events. This step allowed for a deeper understanding of the seismic signature of the most frequently occurring events. However, it is a time-consuming and subjective method when dealing with a high number of detected events.

To address this issue, an automatic cluster analysis (automatic) was carried out using the k-means algorithm, initially using a number of classes equal to 4. However, to achieve a more accurate classification of events, the number of sub-clusters was then further increased to 8. This automated classification method proved to be both efficient and accurate, enabling the fast classification of a large number of events.

Moreover, the analysis of frequency and duration characteristics, as well as the seasonal and hourly occurrence of events in relation to air temperature and precipitation, provided valuable insights into the triggering factors behind these events.

After applying the clustering analysis some of the eight classes (C1 – C8) were merged due to their similarities. As a result, the final classification of events was condensed into four categories:

i. High frequency shallow quakes;
ii. Low frequency deep quakes;
iii. Snow-related events;
iv. Residual hybrid events related to rain and other high-frequency short duration quakes.

In conclusion, the seismic survey conducted on Gran Sometta rock glaciers has provided valuable insights into the dynamics and internal processes of the glaciers.

While this classification approach allows for a more streamlined and efficient analysis of the events, further efforts are still needed to achieve a higher level of precision in detecting and characterizing the origin of these events, including estimating their location.

Overall, seismic monitoring of rock glaciers is an essential tool for understanding their behaviour and mitigation potential hazards associated with them.

BIBLIOGRAPHY

[1] Slides of the course of Innovation Lab for Climate Change

[2] Guillemot, A., Helmstetter, A., Larose, É., Baillet, L., Garambois, S., Mayoraz, R., & Delaloye, R. (2020). Seismic monitoring in the Gugla rock glacier (Switzerland): ambient noise correlation, microseismicity and modelling. Geophysical Journal International, 221(3), 1719-1735.

[3] Roux, P. F., Marsan, D., Métaxian, J. P., O'Brien, G., & Moreau, L. (2008). Microseismic activity within a serac zone in an alpine glacier (Glacier d'Argentiere, Mont Blanc, France). Journal of Glaciology, 54(184), 157-168.

[4] West, M. E., Larsen, C. F., Truffer, M., O'Neel, S., & LeBlanc, L. (2010). Glacier microseismicity. Geology, 38(4), 319-322.

[5] Bearzot, F., Garzonio, R., Di Mauro, B., Colombo, R., Cremonese, E., Crosta, G. B., ... & Rossini, M. (2022). Kinematics of an Alpine rock glacier from multi-temporal UAV surveys and GNSS data. Geomorphology, 402, 108116.

[6] Hibert, C., Mangeney, A., Grandjean, G., Baillard, C., Rivet, D., Shapiro, N. M., ... & Crawford, W. (2014). Automated identification, location, and volume estimation of rockfalls at Piton de la Fournaise volcano. Journal of Geophysical Research: Earth Surface, 119(5), 1082-1105.

[7] Helmstetter, A., & Garambois, S. (2010). Seismic monitoring of Séchilienne rockslide (French Alps): Analysis of seismic signals and their correlation with rainfalls. Journal of Geophysical Research: Earth Surface, 115(F3).

[8] Colombero, C., Comina, C., Vinciguerra, S., & Benson, P. M. (2018). Microseismicity of an unstable rock mass: From field monitoring to laboratory testing. Journal of Geophysical Research: Solid Earth, 123(2), 1673-1693.

[9] Dean, T. (2018). The seismic signature of rain. ASEG Extended Abstracts, 2018(1), 1-8.

[10] Colombero, C., Godio, A., & Jongmans, D. (2021). Ambient seismic noise and microseismicity monitoring of a prone-to-fall quartzite tower (Ormea, NW Italy). Remote Sensing, 13(9), 1664.

[11] Jiang, R., Dai, F., Liu, Y., & Wei, M. (2020). An automatic classification method for microseismic events and blasts during rock excavation of underground caverns. Tunnelling and Underground Space Technology, 101, 103425.

[12] Podolskiy, E. A., Sugiyama, S., Funk, M., Walter, F., Genco, R., Tsutaki, S., ... & Ripepe, M. (2016). Tide-modulated ice flow variations drive seismicity near the calving front of Bowdoin Glacier, Greenland. Geophysical research letters, 43(5), 2036-2044.

[13] Aster, R. C., & Winberry, J. P. (2017). Glacial seismology. Reports on Progress in Physics, 80(12), 126801.

[14] Podolskiy, E. A., Sugiyama, S., Funk, M., Walter, F., Genco, R., Tsutaki, S., ... & Ripepe, M. (2016). Tide-modulated ice flow variations drive seismicity near the calving front of Bowdoin Glacier, Greenland. Geophysical research letters, 43(5), 2036-2044.

[15] Lindner, F., Wassermann, J., & Igel, H. (2021). Seasonal freeze-thaw cycles and permafrost degradation on Mt. Zugspitze (German/Austrian Alps) revealed by single-station seismic monitoring. Geophysical Research Letters, 48(18), e2021GL094659.

[16] Cheng, F., Lindsey, N. J., Sobolevskaia, V., Dou, S., Freifeld, B., Wood, T., ... & Ajo-Franklin, J. B. (2022). Watching the cryosphere thaw: Seismic monitoring of permafrost degradation using distributed acoustic sensing during a controlled heating experiment. Geophysical Research Letters, 49(10), e2021GL097195.

[17] Haeberli, W., Hoelzle, M., Paul, F., & Zemp, M. (2007). Integrated monitoring of mountain glaciers as key indicators of global climate change: the European Alps. Annals of glaciology, 46, 150-160.

[18] Albaric, J., Oye, V., Langet, N., Hasting, M., Lecomte, I., Iranpour, K., ... & Reid, P. (2014). Monitoring of induced seismicity during the first geothermal reservoir stimulation at Paralana, Australia. Geothermics, 52, 120-131.

[19] Stork, A. L., Verdon, J. P., & Kendall, J. M. (2015). The microseismic response at the In Salah Carbon Capture and Storage (CCS) site. International Journal of Greenhouse Gas Control, 32, 159-171.

[20] Withers, M., Aster, R., Young, C., Beiriger, J., Harris, M., Moore, S., & Trujillo, J. (1998). A comparison of select trigger algorithms for automated global seismic phase and event detection. Bulletin of the Seismological Society of America, 88(1), 95-106.

[21] Trnkoczy, A. (2009). Understanding and parameter setting of STA/LTA trigger algorithm. In New manual of seismological observatory practice (NMSOP) (pp. 1-20). Deutsches GeoForschungsZentrum GFZ.

[22] Senfaute, G., Duperret, A., & Lawrence, J. A. (2009). Micro-seismic precursory cracks prior to rock-fall on coastal chalk cliffs: a case study at Mesnil-Val, Normandie, NW France. Natural Hazards and Earth System Sciences, 9(5), 1625-1641.

[23] Na, S., Xumin, L., & Yong, G. (2010, April). Research on k-means clustering algorithm: An improved k-means clustering algorithm. In 2010 Third International

Symposium on intelligent information technology and security informatics (pp. 63-67). Ieee.

[24] Jiang, R., Dai, F., Liu, Y., & Wei, M. (2020). An automatic classification method for microseismic events and blasts during rock excavation of underground caverns. Tunnelling and Underground Space Technology, 101, 103425.

[25] Delaloye, R., Morard, S., Barboux, C., Abbet, D., Gruber, V., Riedo, M., & Gachet, S. (2013). Rapidly moving rock glaciers in Mattertal. Mattertal–ein Tal in Bewegung, edited by: Graf, C., Publikation zur Jahrestagung der Schweizerischen Geomorphologischen Gesellschaft, 29, 21-31.

APPENDICES

APPENDIX A

In this paragraph the time- and frequency-domain parameters used in the clustering analysis for stations GEA3 – GEA5 are shown. The five following figures are related to GEA3 station.

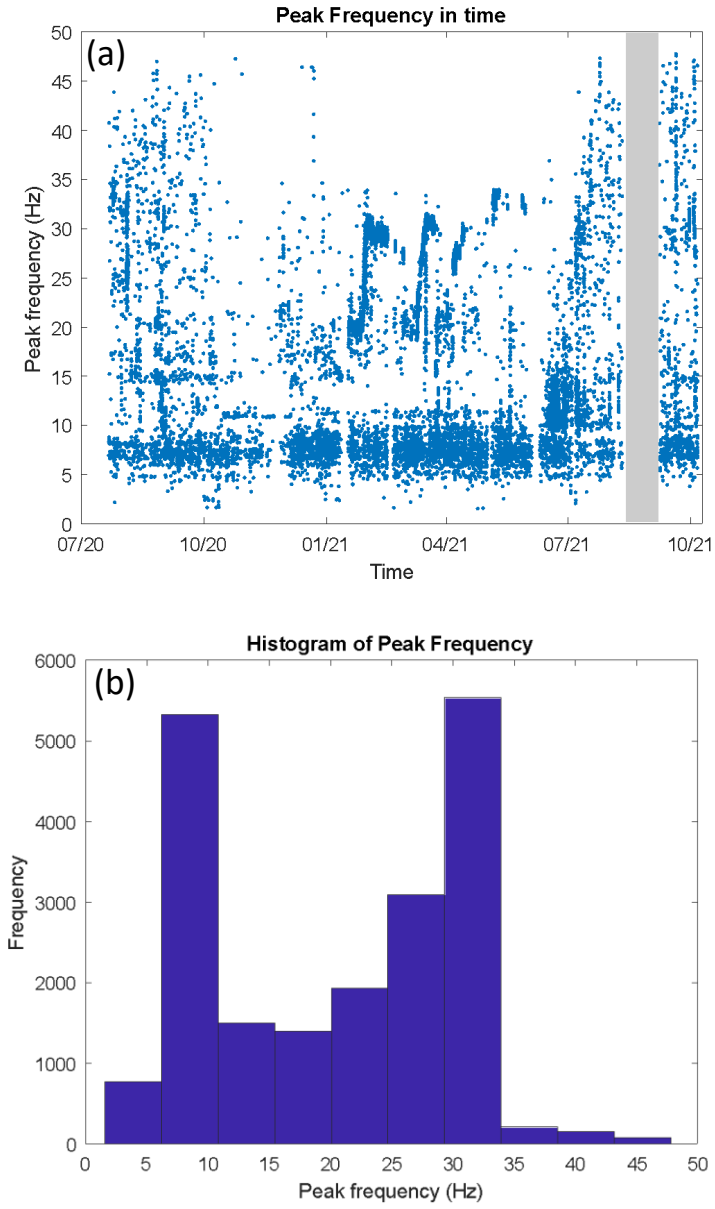

Figure 28. *(a) Peak frequency in time (b) Histogram of peak frequency of GEA3 station's events.*

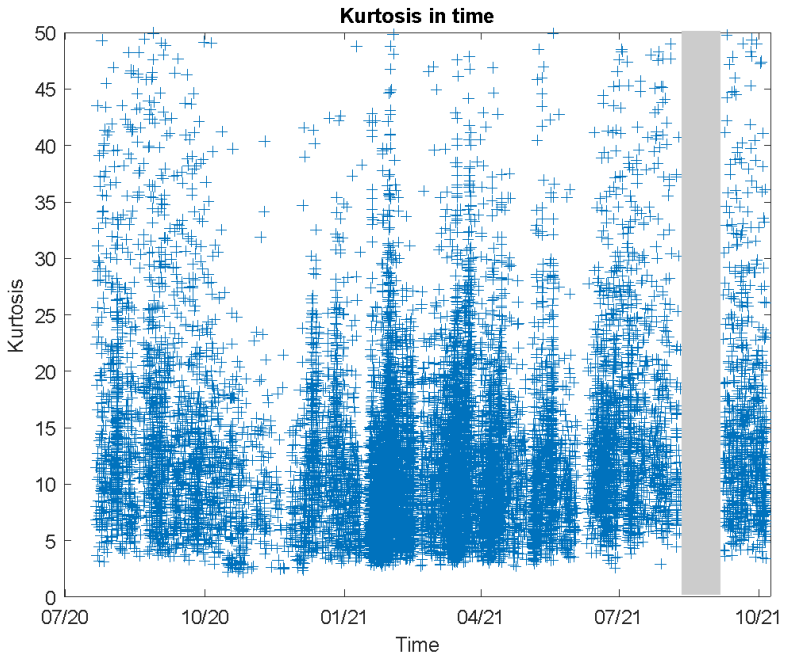

Figure 29. *Kurtosis in time of GEA3 station's events.*

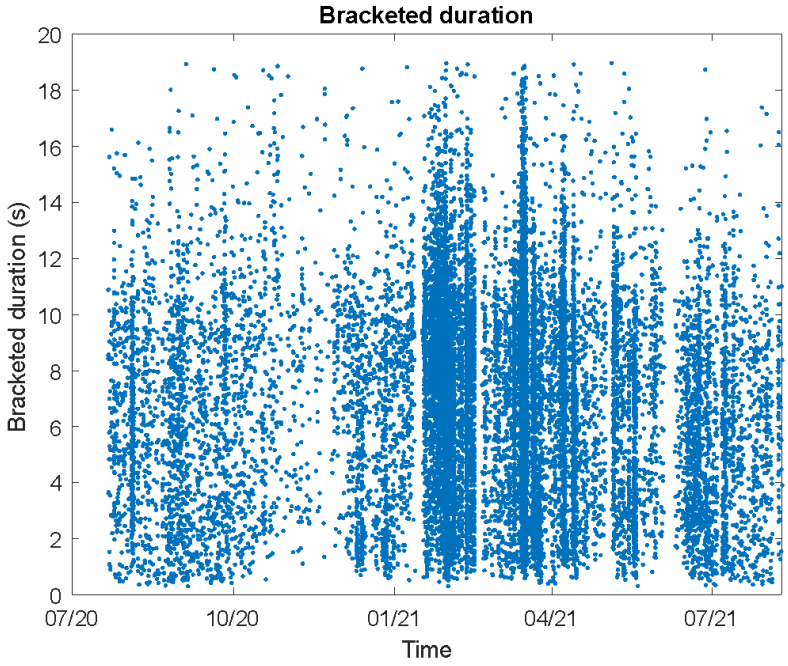

Figure 30. *Temporal evolution of bracketed duration of GEA3 station's events.*

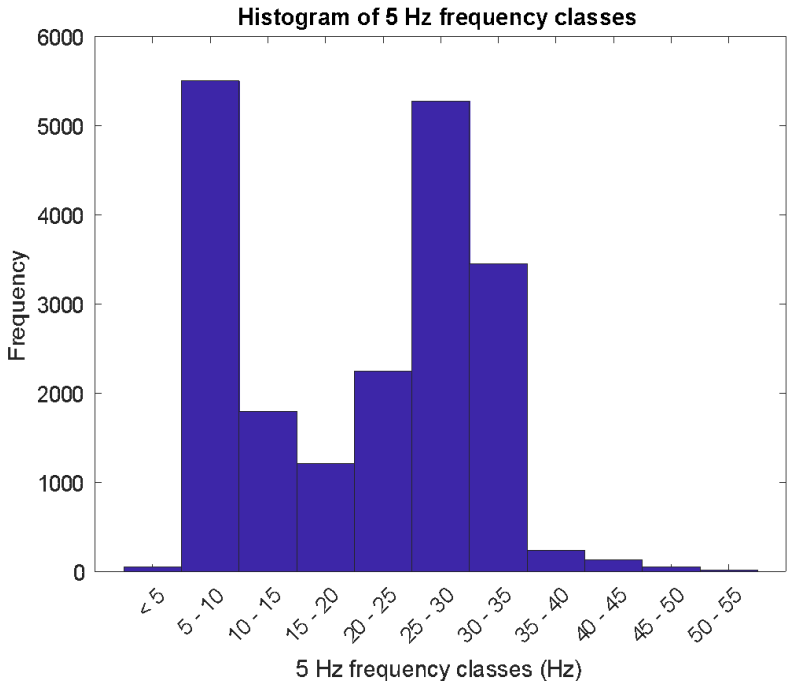

Figure 31. *Histogram of 5-Hz Frequency classes containing the maximum energy amount of GEA3 station's events.*

The events at GEA4 station are characterized by the parameters shown in the following images.

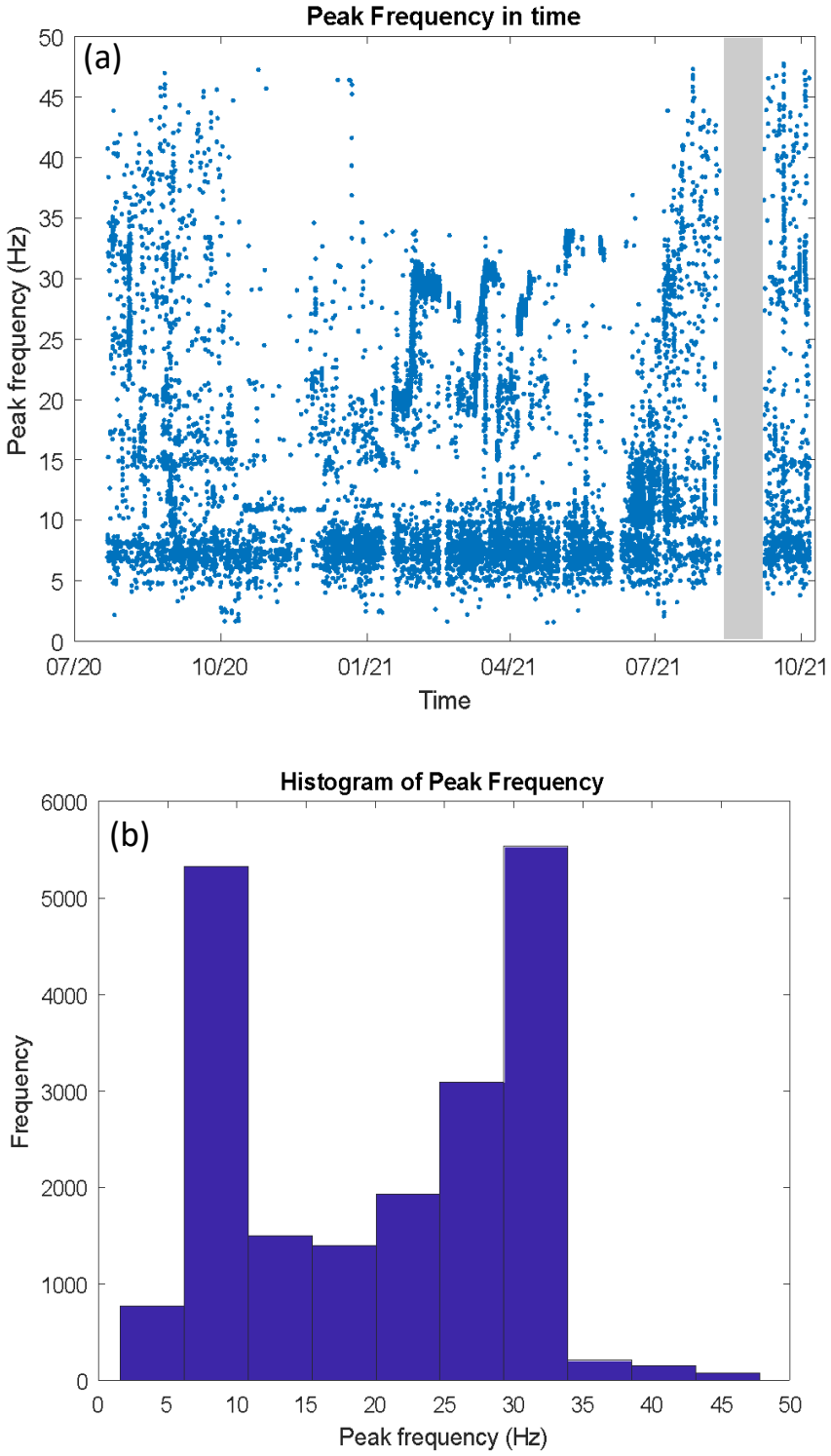

Figure 32. *(a) Peak frequency in time (b) Histogram of peak frequency of GEA4 station's events.*

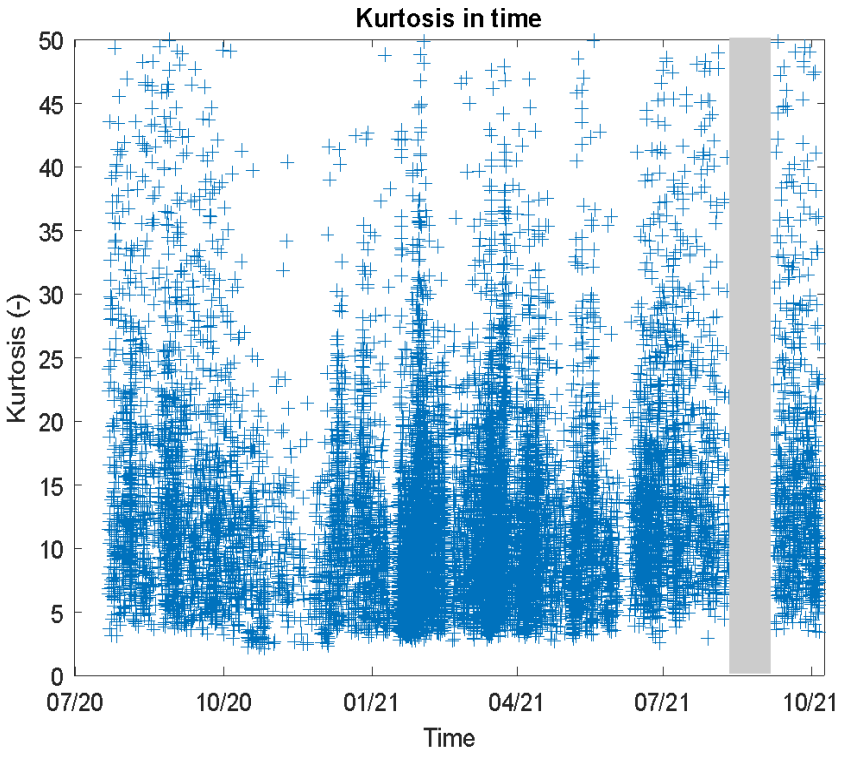

Figure 33. *Kurtosis in time of GEA4 station's events.*

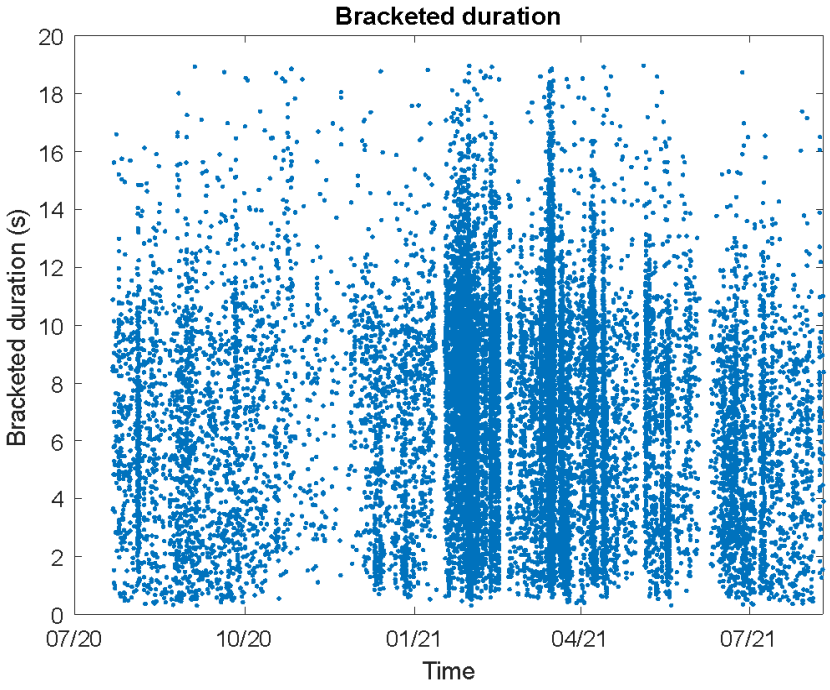

Figure 34. *Bracketed duration in time of GEA4 station's events.*

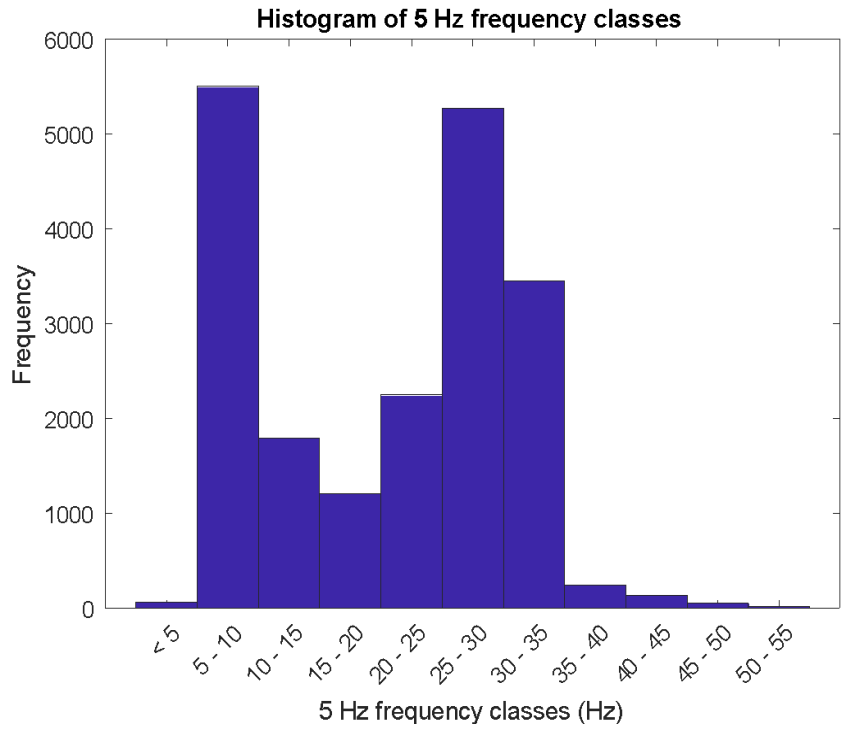

Figure 35. *Histogram of 5-Hz Frequency classes containing the maximum energy amount of GEA4 station's events.*

The following figures show the parameters for the last station, GEA5.

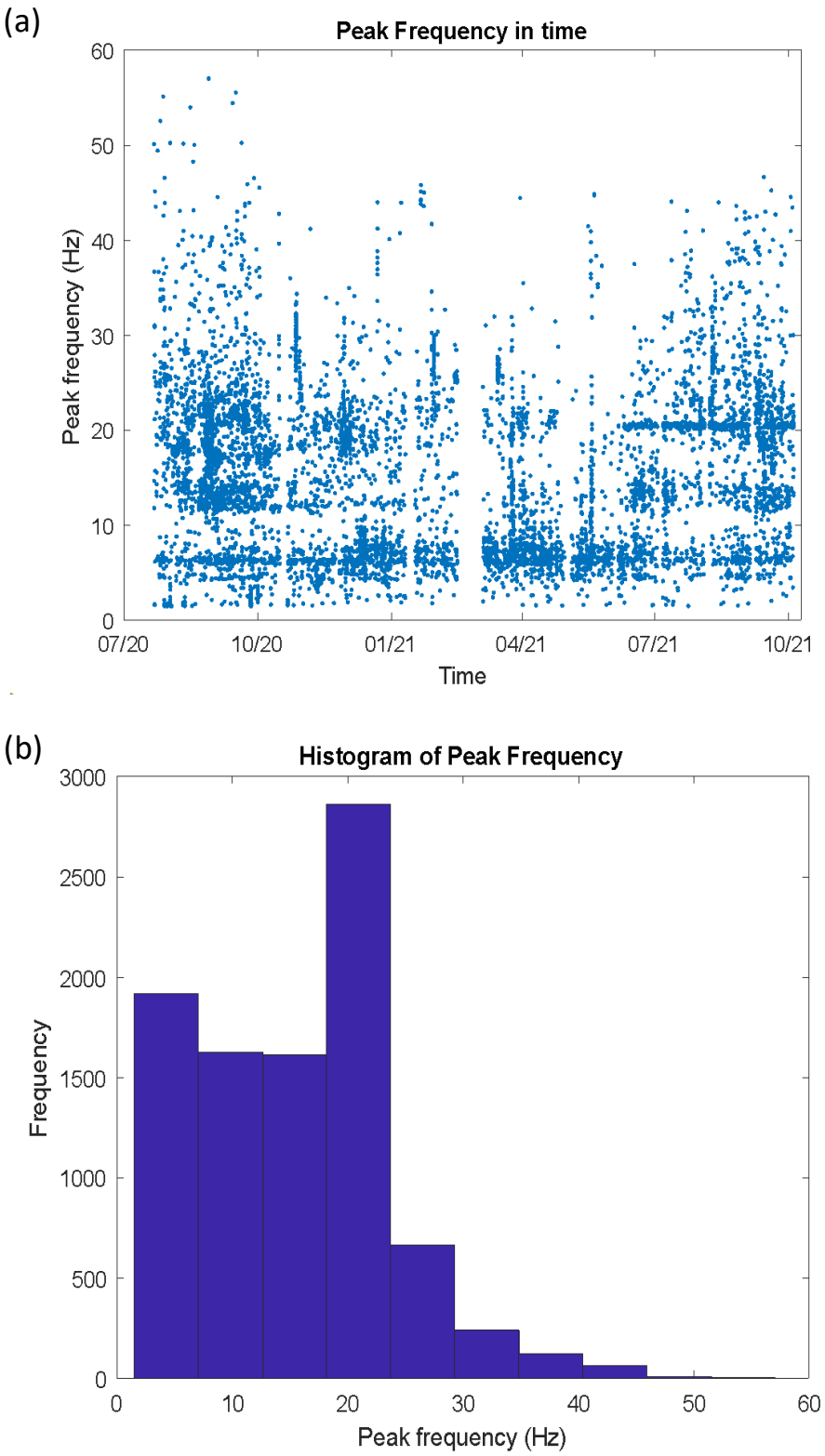

Figure 36. *(a) Peak frequency in time (b) Histogram of peak frequency of GEA5 station's events.*

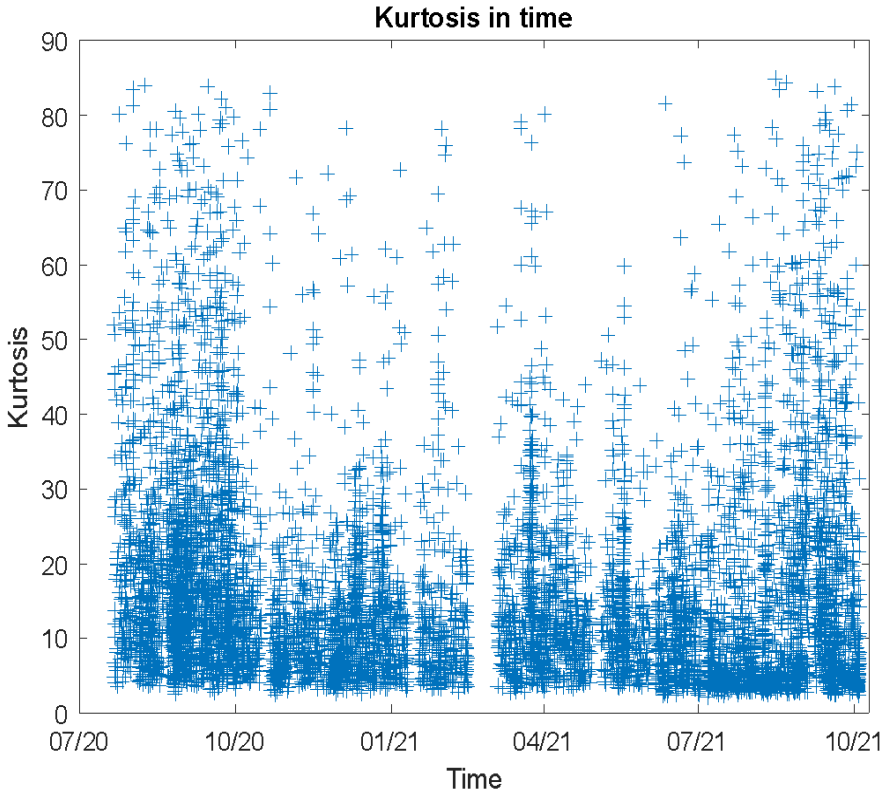

Figure 37. *Kurtosis in time of GEA5 station's events.*

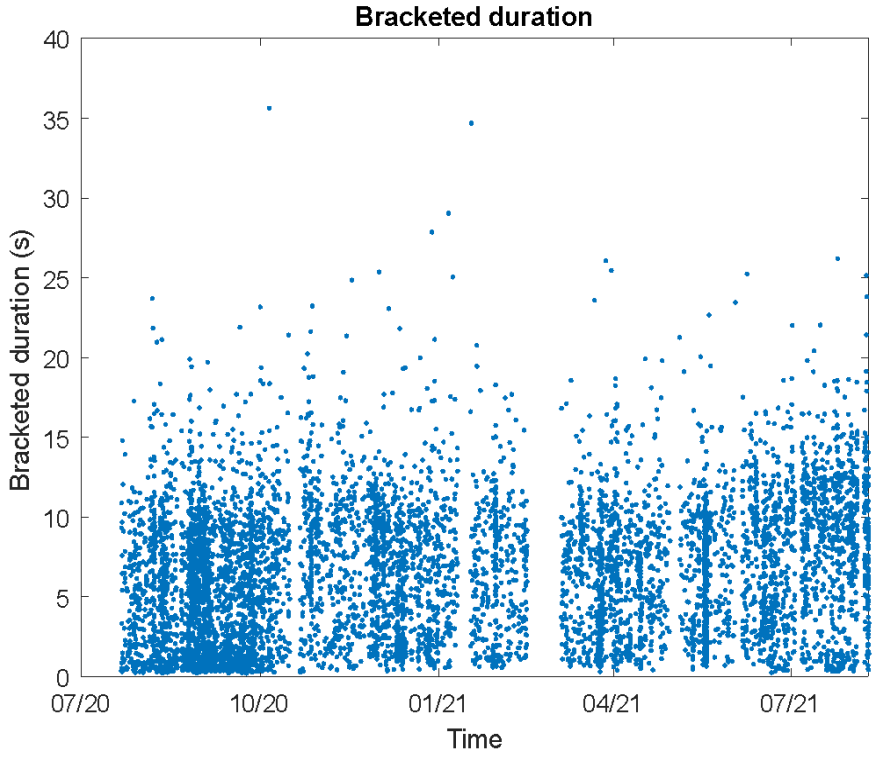

Figure 38. *Bracketed duration in time of GEA5 station's events.*

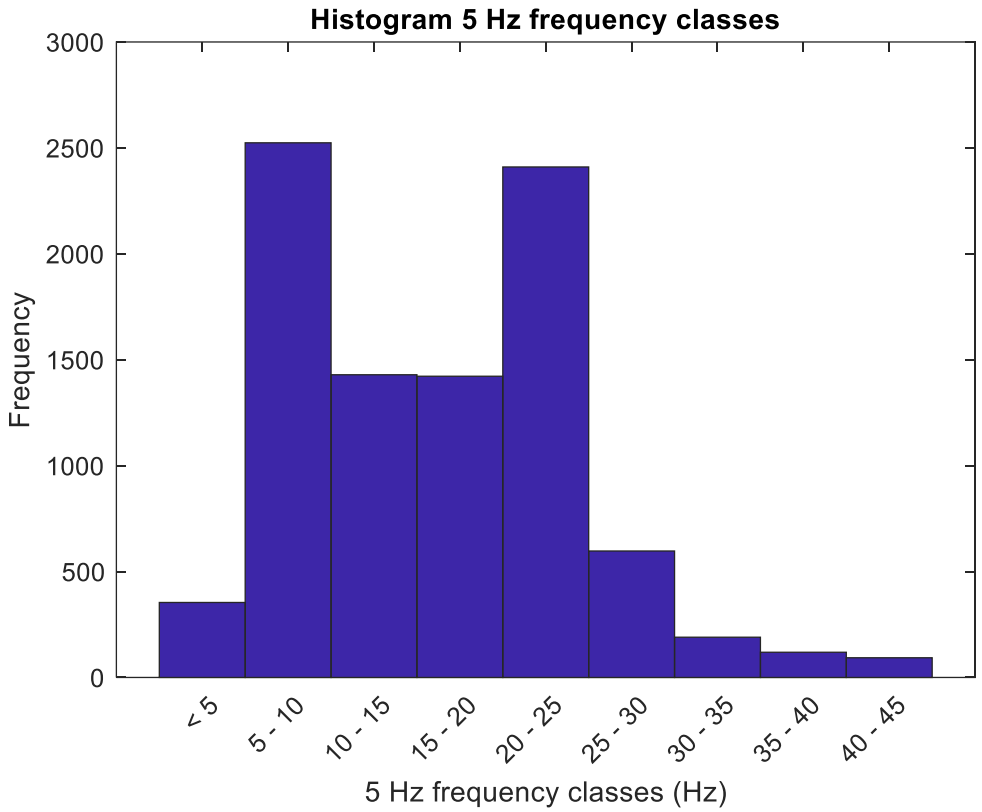

Figure 39. *Histogram of 5-Hz Frequency classes containing the maximum energy amount of GEA5 station's events.*

APPENDIX B

The clustering procedure has been computed also to the other station's events.

Even in this case the clusters were obtained through the application of k-means algorithm on the same four parameters (kurtosis, bracketed duration, 5 Hz frequency classes and peak frequency).

In the following pictures are shown the peak frequency in time of the clustered events and the peak frequency related to the bracketed duration, for each station (GEA3 – GEA5).

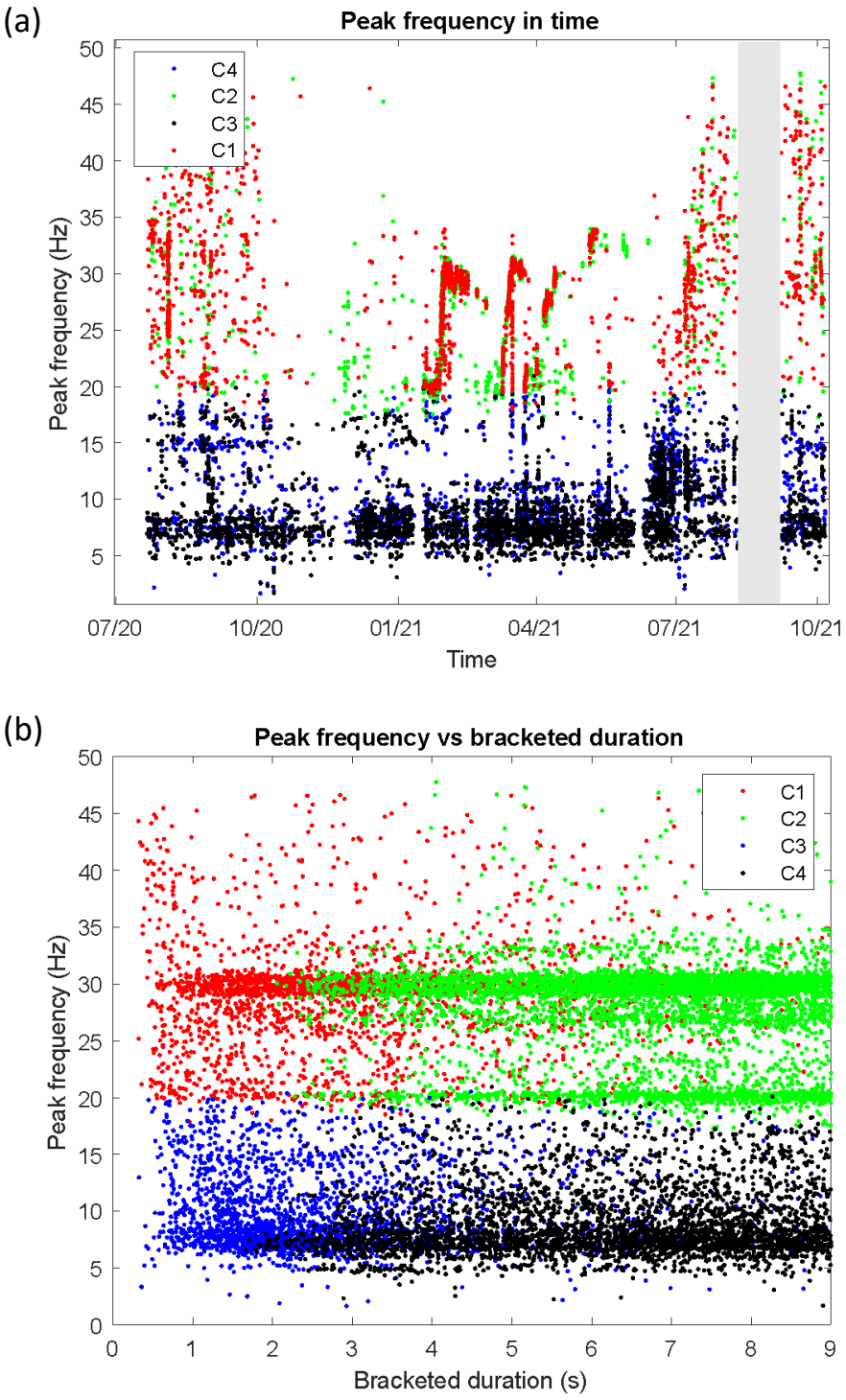

Figure 40. *(a) Peak frequency in time (b) Peak frequency vs bracketed duration of clustering events of GEA3 station.*

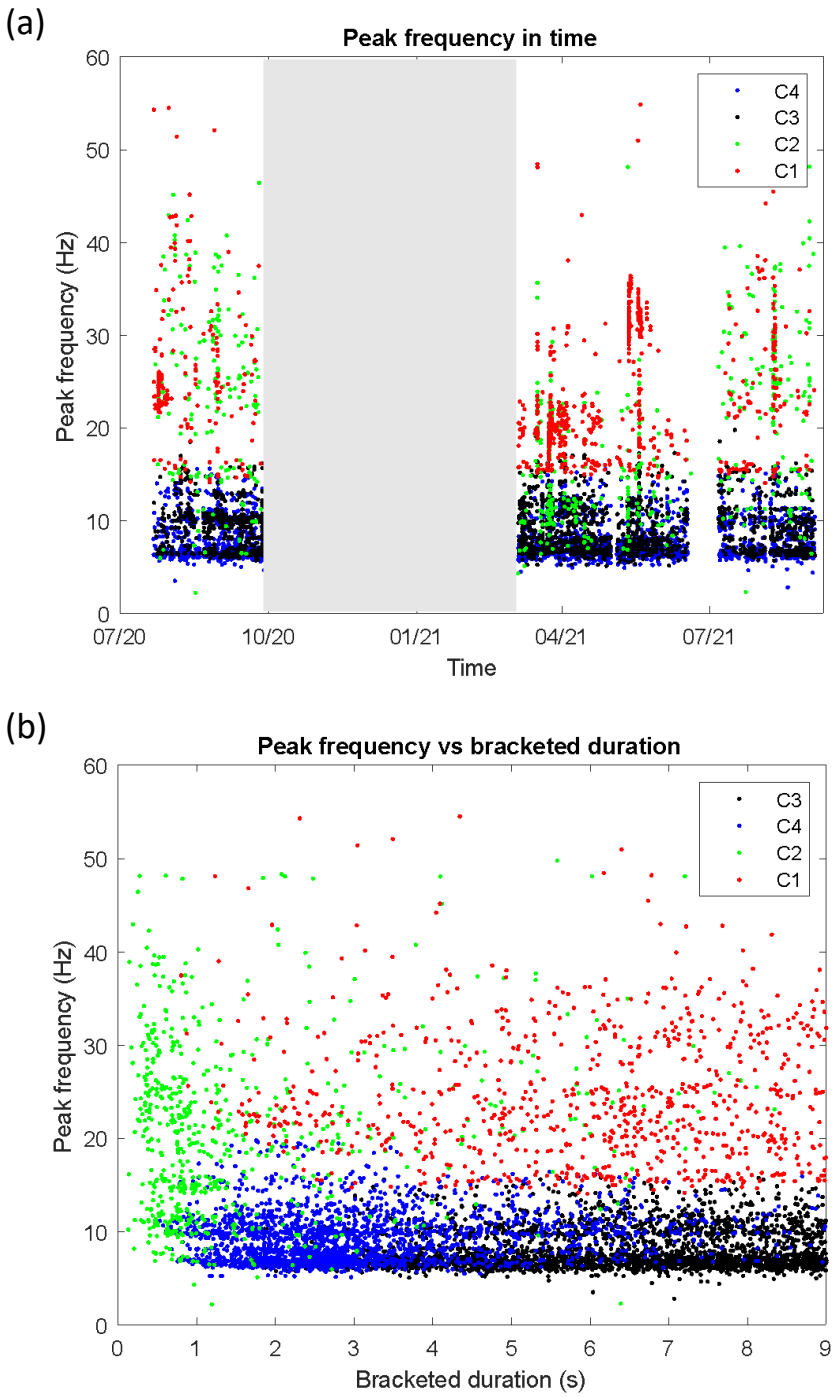

Figure 41. *(a) Peak frequency in time (b) Peak frequency vs bracketed duration of clustering events of GEA4 station.*

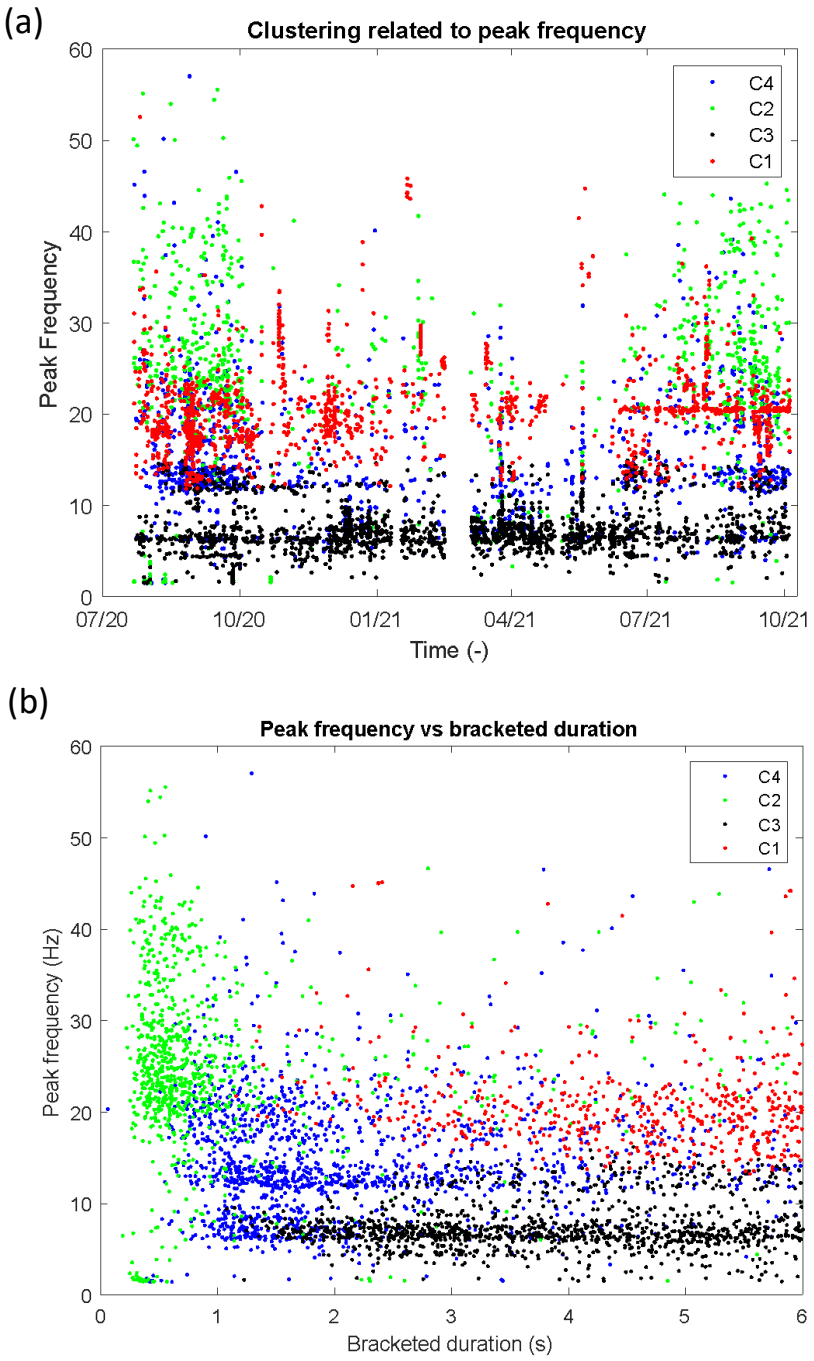

***Figure 42**. (a) Peak frequency in time (b) Peak frequency vs bracketed duration of clustering events of GEA5 station.*